

Reply to the Reviewers: Inter-comparison and improvement of 2-stream shortwave radiative transfer models for unified treatment of cryospheric surfaces in ESMs

Jun 2019

We thank the Editor and two Reviewers for their additional comments. We have addressed the comments raised by the Reviewers as follows:

Anonymous Referee #1

I have examined the manuscript by Dang et al. and my assessment is that the paper would be suitable for publication in The Cryosphere after minor corrections.

The authors have taken away most of the issues raised by the reviewers, and clarified and expanded the paper in a few critical sections.

Remaining minor issues:

line 12: Following reviewer 2, please change "large parts of the Earth" to "mid- and high latitudes."

Fixed.

line 74: ungrammatical: please change to: "... ice is much more absorptive, so that the broadband (or: near-infrared) snow albedo is lower than the visible albedo".

Fixed

line 96: in the literature list, you use Kuipers Munneke et al, but here you use Munneke et al.. Please make consistent.

Fixed

line 114: multi-year snowpack -> a multi-year snowpack

Fixed

line 146: at representing -> for representing

Fixed

line 193: matter of taste but I would say: "where μ is the cosine of the zenith angle"

Fixed

line 226: their algorithms -> its algorithms

Fixed

line 354: to snowpack -> to the snowpack

Fixed

line 433: Please change the order of figure 1 and 2. In the text you present first figure 2 and then 1. Also, Figure 2 would be a more introductory figure, so better to make it figure 1.

We agree that Figure 2 would be a more introductory figure, so we edited the text to cite Figure 2 first, and switched the order of Figures 1 and 2.

line 524: suggest: "Although the differences between algorithms are small, they can have a notable impact on snowpack melt. For example, ..."

Thanks for the suggestion, we have adopted this in the paper.

line 531: self-compensating -> compensating

Fixed

line 569: please avoid this construction with opposing arguments in brackets. It is very confusing. Better: "two-stream models underestimate the column solar absorptions for new snow, and they overestimate them for old snow. ..."

Fixed

line 594: within snowpack -> within the snowpack

Fixed

line 595: among three two-stream models -> among the three two-stream models.

Fixed

line 603: Break up this sentence into two sentences.

Fixed

line 624: I assume that this correction is applied only for theta > 75 degrees. Please add this in the formula (for theta > 75 deg)

We have edited Equation 12 to indicate this condition, which also applies to equations 14 (a) and (b).

$$R_{75+} = \frac{\alpha_{16-DISORT}}{\alpha_{dEdD-AD}} = c_1(\mu_0) \log_{10}(r) + c_0(\mu_0), \text{ for } \mu_0 < 0.26, \text{ i.e. } \theta_0 > 75^\circ \quad (12)$$

line 654: surface of snowpack -> surface of the snowpack

Fixed

line 663: suggest "Although the errors of direct near-IR albedos...."

Fixed

line 666: can be important at/for high latitudes.

Fixed

line 667: remains large -> is large
Fixed

line 672: broader band-averaged. Please use consistent terms. Replace by "narrowband-averaged" or "band-averaged".
Fixed

line 755: Replace the term "discussion" by "proposal for" or "requirements for" or "towards" or "designing".
We have replaced "discussion" with "towards". Thank you for this suggestion.

line 787: suggest "Third, in a cryospheric radiative transfer model, one should prefer ..."
Fixed

line 839: Adopting dEdd-AD radiative core -> Adopting the dEdd-AD radiative core
Fixed

Referee #2
David Bailey (dbailey@ucar.edu)

The authors have generally addressed my concerns from my first review. I still do not like the first sentence of the abstract: "Snow is an important climate regulator because it greatly increases the surface albedo of large parts of the Earth." I am thinking something more like "15% or 20% of the Earth". It still kind of lacks in motivation, however the manuscript is generally fine and would be of interest to the readers of the Cryosphere.

Thank you. We have revised the abstract to:

Lines 11: "Snow is an important climate regulator because it greatly increases the surface albedo of middle and high latitudes of the Earth. Earth System Models (ESMs) often adopt two-stream approximations with different radiative transfer techniques, the same snow therefore has different solar radiative properties depending whether it is on land or on sea ice..."

1 **Inter-comparison and improvement of two-stream shortwave radiative transfer**
2 **models in ESMs for a unified treatment of cryospheric surfaces**
3

4 Cheng Dang¹, Charles S. Zender¹, Mark G. Flanner²
5

6 ¹ Department of Earth System Science, University of California, Irvine, CA, USA

7 ² Department of Climate and Space Sciences and Engineering, University of Michigan,
8 Ann Arbor, MI, USA

9 *Correspondence to:* Cheng Dang (cdang5@uci.edu)

10
11 **Abstract.** Snow is an important climate regulator because it greatly increases the surface
12 albedo of middle and high latitudes of the Earth. Earth System Models (ESMs) often
13 adopt two-stream approximations with different radiative transfer techniques, the same
14 snow therefore has different solar radiative properties depending whether it is on land or
15 on sea ice. Here we inter-compare three two-stream algorithms widely used in snow
16 models, improve their predictions at large zenith angles, and introduce a hybrid model
17 suitable for all cryospheric surfaces in ESMs. The algorithms are those employed by the
18 SNow ICe and Aerosol Radiative (SNICAR) module used in land models, and by dEdd-
19 AD used in Icepack, the column physics used in the Los Alamos sea ice model CICE and
20 MPAS-seaice, and a two-stream discrete ordinate (2SD) model. Compared with a 16-
21 stream benchmark model, the errors in snow visible albedo for a direct-incident beam
22 from all three two-stream models are small ($< \pm 0.005$) and increase as snow shallows,
23 especially for aged snow. The errors in direct near-infrared (near-IR) albedo are small
24 ($< \pm 0.005$) for solar zenith angles $\theta < 75^\circ$, and increase as θ increases. For diffuse
25 incidence under cloudy skies, dEdd-AD produces the most accurate snow albedo for both
26 visible and near-IR ($< \pm 0.0002$) with the lowest underestimate (-0.01) for melting thin
27 snow. SNICAR performs similarly to dEdd-AD for visible albedos, with a slightly larger
28 underestimate (-0.02), while it overestimates the near-IR albedo by an order of magnitude
29 more (up to 0.04). 2SD overestimates both visible and near-IR albedo by up to 0.03. We
30 develop a new parameterization that adjusts the underestimated direct near-IR albedo and
31 overestimated direct near-IR heating persistent across all two-stream models for $\theta > 75^\circ$.
32 These results are incorporated in a hybrid model SNICAR-AD, which can now serve as a
33 unified solar radiative transfer model for snow in ESM land, land ice, and sea-ice
34 components.
35

Author 7/8/19 8:01 PM

Deleted: Snow is an important climate regulator because it greatly increases the surface albedo of . Earth System Models (ESMs) often adopt two-stream approximations with different radiative transfer techniques, the same snow therefore has different solar radiative properties depending whether it is on land or on sea ice.

Author 7/14/19 8:35 PM

Deleted: solar zenith angles

Author 7/8/19 8:01 PM

Formatted: Font:Not Bold, Underline color: Blue

45 **1. Introduction**

46
47 Snow cover on land, land ice, and sea ice, modulates the surface energy balance of
48 middle and high latitudes of the Earth, principally because even a thin layer of snow can
49 greatly increase the surface albedo. Integrated over the solar spectrum, the broadband
50 albedo of opaque snow ranges from 0.7 – 0.9 (e.g., Wiscombe and Warren 1980; Dang et
51 al., 2015). In contrast, the albedo of other natural surfaces is smaller: 0.2, 0.25, and 0.5-
52 0.7 for damp soil, grassland, and bare multi-year sea ice, respectively (Perovich 1996;
53 Liang et al., 2002; Brandt et al., 2005; Bøggild et al., 2010). The accumulation, evolution,
54 and depletion of snow cover thus modify the seasonal cycle of surface albedo globally. In
55 particular, snow over sea ice absorbs more solar energy and begins to melt in the spring,
56 which forms melt ponds that bring the sea-ice albedo to as low as 0.15 to further
57 accelerate ice melt (Light et al., 2008, 2015). An accurate simulation of the shortwave
58 radiative properties of snowpack is therefore crucial for spectrally partitioning solar
59 energy and representing snow-albedo feedbacks across the Earth system. Unfortunately,
60 computational demands and coupling architectures often constrain representation of
61 snowpack radiative processes in Earth System Models (ESMs, please refer to Table 1 for
62 all acronyms used in this work) to relatively crude approximations such as two-stream
63 methods (Wiscombe and Warren, 1980, Toon et al., 1989). In this work, we inter-
64 compare two-stream methods widely used in snow models and then introduce a new
65 parameterization that significantly reduces their snowpack reflectance and heating biases
66 at large zenith angles, to produce more realistic behavior in polar regions.

67
68 Snow albedo is determined by many factors including the snow grain radius, the solar
69 zenith angle, cloud transmittance, light-absorbing particles, and the albedo of underlying
70 ground if snow is optically thin (Wiscombe and Warren, 1980; Warren and Wiscombe,
71 1980); it also varies strongly with wavelength since the ice absorption coefficient varies
72 by 7 orders of magnitudes across the solar spectrum (Warren and Brandt, 2008). At
73 visible wavelengths (0.2 - 0.7 μm), ice is almost non-absorptive such that the absorption
74 of visible energy by snowpack is mostly due to the light-absorbing particles (e.g. black
75 carbon, organic carbon, mineral dust) that were incorporated during ice nucleation in
76 clouds, scavenged during precipitation, or slowly sedimented from the atmosphere by
77 gravity (Warren and Wiscombe, 1980, 1985; Doherty et al., 2010, 2014, 2016; Wang et
78 al., 2013; Dang and Hegg 2014). As snow becomes shallower, visible photons are more
79 likely to penetrate through snowpack and get absorbed by darker underlying ground. At
80 near-infrared (near-IR) wavelengths (0.7 – 5 μm), ice is much more absorptive, so that

Author 6/28/19 1:18 PM

Deleted:

Author 6/28/19 1:18 PM

Deleted: snow

Author 6/28/19 10:00 PM

Deleted: parameterization

82 | the snow near-IR albedo is lower than the visible albedo. Larger ice crystals form a lower
83 | albedo surface than smaller ice crystals hence aged snowpacks absorb more solar energy.
84 | Photons incident at smaller solar zenith angles are more likely to penetrate deeper
85 | vertically and be scattered in the snowpack until being absorbed by the ice/the underlying
86 | ground/absorbing impurities, which also leads to a smaller snow albedo. To compute the
87 | reflected solar flux, spectrally resolved albedo must be weighted by the incident solar
88 | flux, which is mostly determined by solar zenith angle, cloud cover and transmittance,
89 | and column water vapor. Modeling the solar properties of snowpacks must consider the
90 | spectral signatures of these atmospheric properties.

91 |
92 | Several parameterizations have been developed to compute the snow solar properties
93 | without solving the radiative transfer equations and some are incorporated into ESMs or
94 | regional models. Marshall and Warren (1987) and Marshall (1989) parameterized snow
95 | albedo in both visible and near-IR bands as functions of snow grain size, solar zenith
96 | angle, cloud transmittance, snow depth, underlying surface albedo, and black carbon
97 | content. Marshall and Oglesby (1994) used this in an ESM. Gardner and Sharp (2010)
98 | computed the all-wave snow albedo with similar inputs. This was incorporated into the
99 | regional climate model RACMO

100 | (<https://www.projects.science.uu.nl/iceclimate/models/racmo.php>) to simulate snow
101 | albedo in glaciated regions like Antarctica and Greenland (Kuipers Munneke et al.,
102 | 2011). Dang et al., (2015) parameterized snow albedo as functions of snow grain radius,
103 | black carbon content, and dust content for visible and near-IR bands and 14 narrower
104 | bands used in the rapid radiative transfer model (RRTM, Mlawer and Clough, 1997).
105 | Their algorithm can also be expanded to different solar zenith angles using the zenith
106 | angle parameterization developed by Marshall and Warren (1987). Aoki et al., (2011)
107 | developed a more complex model based on the offline snow albedo and a transmittance
108 | look-up table. This can be applied to multilayer snowpack to compute the snow albedo
109 | and the solar heating profiles as functions of snow grain size, black carbon and dust
110 | content, snow temperature, and snowmelt water equivalent. These parameterizations are
111 | often in the form of simplified polynomial equations, which are especially suitable to
112 | long-term ESM simulations that require less time-consuming snow representations.

113 |
114 | More complex models that explicitly solve the multiple scattering radiative transfer
115 | equations have also been developed to compute snow solar properties. Flanner and
116 | Zender (2005) developed the SNow Ice and Aerosol Radiation model (SNICAR) that
117 | utilizes two-stream approximations (Wiscombe and Warren 1980; Toon et al., 1989) to

120 | predict heating and reflectance for a multi-layer snowpack. They implemented SNICAR
121 | in the Community Land Model (CLM) to predict snow albedo and vertically resolved
122 | solar absorption for snow-covered surfaces. Before SNICAR, CLM prescribed snow
123 | albedo and confined all solar absorption to the top snow layer (Flanner and Zender 2005).
124 | Over the past decades, updates and new features have been added to SNICAR to consider
125 | more processes such as black carbon/ice mixing states (Flanner et al., 2012) and snow
126 | grain shape (He et al., 2018b). Concurrent with the development of SNICAR, Briegleb
127 | and Light (2007) improved the treatment of sea-ice solar radiative calculations in
128 | Community Climate System Model (CCSM). They implemented a different two-stream
129 | scheme with delta-Eddington approximation and adding-doubling technique (hereafter,
130 | dEdd-AD) that allows CCSM to compute bare/ponded/snow-covered sea ice albedo and
131 | solar absorption profiles of multi-layer sea ice. Before these improvements, the sea-ice
132 | albedo was computed based on surface temperature, snow thickness, and sea-ice
133 | thickness using averaged sea ice and snow albedo. dEdd-AD has been adopted by the
134 | sea-ice physics library Icepack (<https://github.com/CICE-Consortium/Icepack/wiki>),
135 | which is used by the Los Alamos Sea Ice Model CICE (Hunke et al., 2010) and Model for
136 | Prediction Across Scales Sea Ice MPAS-seaice (Turner et al., 2018). CICE itself is used
137 | in numerous global and regional models.

138

139 | SNICAR and dEdd-AD solve the multiple scattering radiative transfer equations and
140 | provide much improved solar radiative representations for the cryosphere, though their
141 | separate development and implementation created an artificial divide for snow
142 | simulation. In ESMs that utilize both SNICAR and dEdd-AD, such as the Community
143 | Earth System Model (CESM, <http://www.cesm.ucar.edu/>) and the Energy Exscale Earth
144 | System Model (E3SM, previously known as ACME, <https://e3sm.org/>), the solar
145 | radiative properties of snow on land and snow on sea ice are computed separately via
146 | SNICAR and dEdd-AD. As a result, the same snow in nature has different solar radiative
147 | properties such as reflectance depending on which model represents it. These differences
148 | are model artifacts that should be eliminated so that snow has consistent properties across
149 | the Earth system.

150

151 | In this paper, we evaluate the accuracy and biases of three two-stream models listed in
152 | Table 2, including the algorithms used in SNICAR and dEdd-AD, for representing
153 | reflectance and heating. In Sections 2-4, we describe the radiative transfer algorithms and
154 | calculations performed in this work. The results and model inter-comparisons are
155 | discussed in Section 5. In Section 6, we introduce a parameterization to reduce the

Author 6/28/19 3:13 PM

Deleted: at

157 simulated albedo and heating bias for solar zenith angles larger than 75°. In Section 7, we
158 summarize the major differences of algorithm implementations between SNICAR and
159 dEdd-AD in ESMs. We use these results to develop and justify a unified surface
160 shortwave radiative transfer method for all Earth system model components in the
161 cryosphere, presented in Section 8.

162

163 2. Radiative Transfer Model

164

165 In this section, we summarize the three two-stream models and the benchmark DISORT
166 model with 16-streams. These algorithms are well documented in papers by Toon et al.,
167 (1989), Briegleb and Light (2007), Jin and Stamnes (1994), and Stamnes et al. (1988).
168 Readers interested in detailed mathematical derivations should refer to those papers. We
169 only include their key equations to illustrate the difference among two-stream models for
170 discussion purposes.

171

172 2.1 SNICAR in land models CLM and ELM

173 SNICAR is implemented as the default snow shortwave radiative transfer scheme in
174 CLM and E3SM land model (ELM). It adopts the two-stream algorithms and the rapid
175 solver developed by Toon et al., (1989) to compute the solar properties of multi-layer
176 snowpacks. These two-stream algorithms are derived from the general equation of
177 radiative transfer in a plane parallel media:

178

$$179 \mu \frac{\partial I}{\partial \tau}(\tau, \mu, \Phi) = I(\tau, \mu, \Phi) - \frac{\varpi}{4\pi} \int_0^{2\pi} \int_{-1}^1 P(\mu, \mu', \phi, \phi') I(\tau, \mu', \Phi') d\mu' d\phi' - S(\tau, \mu, \Phi)$$

180
181 (1)
182
183

184 where Φ is azimuth angle, μ is the cosine of the zenith angle, ϖ is single-scattering
185 albedo. On the right-hand side, the three terms are intensity at optical depth τ , internal
186 source term due to multiple scattering, and external source term S . For a purely external
187 source at solar wavelengths S is:

188

$$189 S = \frac{\varpi}{4} F_s P(\mu, -\mu_0, \phi, \phi_0) \exp\left(\frac{-\tau}{\mu_0}\right)$$

190 (2)

191

191 where πF_s is incident solar flux, μ_0 is the incident direction of the solar beam. Integrating
192 equation (1) over azimuth and zenith angles yields the general solution of two-stream

Author 6/28/19 10:02 PM
Deleted: arccos(μ) and
Author 6/28/19 10:02 PM
Deleted: are
Author 6/28/19 10:02 PM
Deleted: zenith angle and

196 approximations (Meador and Weaver, 1980). The upward and downward fluxes at optical
197 depth τ of layer n can be represented as:

198

199

$$200 F_n^+ = k_{1n} \exp(\Lambda_n \tau) + \Gamma_n k_{2n} \exp(-\Lambda_n \tau) + C_n^+(\tau) \quad (3a)$$

201

$$202 F_n^- = \Gamma_n k_{1n} \exp(\Lambda_n \tau) + k_{2n} \exp(-\Lambda_n \tau) + C_n^-(\tau) \quad (3b)$$

203

204

205 where Λ_n , Γ_n , C_n are known coefficients determined by the two-stream method, incident
206 solar flux, and solar zenith angle; whereas k_{1n} and k_{2n} are unknown coefficients
207 determined by the boundary conditions. For an N-layer snowpack, the solutions for
208 upward and downward fluxes are coupled at layer interfaces to generate 2N equations
209 with 2N unknown coefficients k_{1n} and k_{2n} . Combining these equations linearly generates
210 a new set of equations with terms in tridiagonal form that enables the application of a fast
211 tri-diagonal matrix solver. With the solved coefficients, the upward and downward fluxes
212 are computed at different optical depths (Equations 3a and 3b) and eventually the
213 reflectance, transmittance, and absorption profiles of solar flux for any multilayer
214 snowpack.

215

216 SNICAR itself implements all three two-stream algorithms in Toon et al., (1989):
217 Eddington, Quadrature, and Hemispheric-mean. In practical simulations, it utilizes the
218 Eddington and Hemispheric-mean approximations to compute the visible and near-IR
219 snow properties, respectively (Flanner et al., 2007). In addition to [jts](#) algorithms,
220 SNICAR implements the Delta-transform of the fundamental input variables asymmetry
221 factor (g), single-scattering albedo (ω), and optical depth (τ) to account for the strong
222 forward scattering in snow (Equations 2 (a)-(c), Wiscombe and Warren, 1980).

223

224 2.2. dEdd-AD in sea ice models Icepack, CICE, and MPAS-seaice

225 Icepack, CICE, and MPAS-seaice use the same shortwave radiative scheme dEdd-AD
226 developed and documented by Briegleb and Light (2007). Sea ice is divided into multiple
227 layers to first compute the single-layer reflectance and transmittance using two-stream
228 delta-Eddington solutions to account for the multiple scattering of light within each layer
229 (Equation set 50, Briegleb and Light, 2007), where the name “delta” implies dEdd-AD
230 implements the Delta-transform to account for the strong forward scattering of snow and

Author 6/28/19 3:17 PM

Deleted: their

232 sea ice (Equations 2 (a)-(c), Wiscombe and Warren, 1980). The single-layer direct albedo
233 and transmittance are computed by equations:

234

$$235 \quad R(\mu_{0,n}) = A_n \exp\left(\frac{-\tau}{\mu_{0,n}}\right) + B_n(\exp(\varepsilon_n \tau) - \exp(-\varepsilon_n \tau)) - K_n \quad (4a)$$

236

$$237 \quad T(\mu_{0,n}) = E_n + H_n(\exp(\varepsilon_n \tau) - \exp(-\varepsilon_n \tau)) \exp\left(\frac{-\tau}{\mu_{0,n}}\right) \quad (4b)$$

238

239 where coefficients A_n , B_n , K_n , E_n , H_n , and ε_n are determined by the single-scattering
240 albedo (ω), asymmetry factor (g), optical depth (τ), and angle of the incident beam at
241 layer n ($\mu_{0,n}$). Following the delta-Eddington assumption, simple formulas are available
242 for the single-layer reflectance and transmittance under both clear sky (direct flux,
243 equations 4a and 4b) and overcast sky (diffuse flux) conditions, however, the formula
244 derived by applying diffuse-flux upper boundary conditions sometimes yields negative
245 albedos (Wiscombe 1977). To avoid the unphysical values, diffuse reflectance \bar{R} and
246 transmittance \bar{T} of a single layer are computed by integrating the direct reflectance $R(\mu)$
247 and transmittance $T(\mu)$ over the incident hemisphere assuming isotropic incidence:

248

$$249 \quad \bar{R} = 2 \int_0^1 \mu R(\mu) d\mu \quad (5a)$$

250

$$251 \quad \bar{T} = 2 \int_0^1 \mu T(\mu) d\mu \quad (5b)$$

252

253 This is the same as the method proposed by Wiscombe and Warren (1980, their equation
254 5). In practice, eight Gaussian angles are implemented to perform the integration for
255 every layer.

256

257 The computed single-layer reflectance and transmittance of direct and diffuse
258 components are then combined to account for the inter-layer scattering of light to
259 compute the reflectance and transmission at every interface (Equation set 51, Briegleb
260 and Light, 2007), and eventually the upward and downward fluxes (Equation set 52,
261 Briegleb and Light, 2007). These upward and downward fluxes at each optical depth are
262 then used to compute the column reflectance and transmittance, and the absorption
263 profiles for any multilayered media, such as snowpacks on land and sea ice.

264

265 In nature, a large fraction of sea ice is covered by snow during winter. As snow melts
266 away in late spring and summer, it exposes bare ice, and melt ponds form on the ice

267 surface. Such variation of sea-ice surface types requires the shortwave radiative transfer
 268 model to be flexible and capable of capturing the light refraction and reflection.
 269 Refractive boundaries exist where air (refractive index $m_{re} = 1.0$), snow (assuming snow
 270 as medium of air containing a collection of ice particles, $m_{re} = 1.0$), pond (assuming pure
 271 water, $m_{re} = 1.33$), and ice (assuming pure ice, $m_{re} = 1.31$) are present in the same sea-ice
 272 column. The general solution of delta-Eddington, and the two-stream algorithms used in
 273 SNICAR are not applicable to such non-uniformly refractive layered media. To include
 274 the effects of refraction, Briegleb and Light (2007) modified the adding formula at the
 275 refractive boundaries (i.e. interfaces between air/ice, snow/ice, air/pond). The reflectance
 276 and transmittance of the adjacent layers above and below the refractive boundary are
 277 combined with modifications to include the Fresnel reflection and refraction of direct and
 278 diffuse fluxes (Section 4.1, Briegleb and Light, 2007). dEdd-AD can thus be applied to
 279 any layered media with either uniform (e.g., snow on land) or non-uniform (e.g., snow on
 280 sea ice) refractive indexes.

281
 282 In this paper, we apply dEdd-AD to snowpacks that can be treated as uniform refractive
 283 media such as the air/snowpack/land columns assumed in SNICAR for model evaluation.
 284 An ideal radiative treatment for snow should, however, keep the potential to include
 285 refraction for further applications to snow on sea ice or ice sheets. Therefore, besides
 286 these two widely used algorithms in Icepak and SNICAR, we evaluate a third algorithm
 287 (section 2.3) that can be applied to layered media with either uniform or non-uniform
 288 refractive indexes.

289
 290 2.3. two-stream discrete-ordinate algorithm (2SD)
 291 A refractive boundary also exists between the atmosphere and the ocean, and models
 292 have been developed to solve the radiative transfer problems in the atmosphere-ocean
 293 system using the discrete-ordinate technique (e.g. Jin and Stamnes, 1994; Lee and Liou,
 294 2007). Similar to the two-stream algorithms of Toon et al., (1989) used in SNICAR, Jin
 295 and Stamnes (1994) also developed their algorithm from the general equation:

296
 297
$$\mu \frac{\partial I}{\partial \tau}(\tau, \mu) = I(\tau, \mu) - \frac{\omega}{4\pi} \int_{-1}^1 P(\tau, \mu, \mu') I(\tau, \mu') d\mu' - S(\tau, \mu) \quad (6)$$

 298

299 Equation (6) is the azimuthally integrated version of equation (1). However, for vertically
 300 inhomogeneous media like the atmosphere-ocean or sea ice, the external source term
 301 $S(\tau, \mu)$ is different. Specifically, for the medium of total optical depth τ^a above the

302 refractive interface, one must consider the contribution from the upward beam reflected
 303 at the refractive boundary (second term on the right-hand side):

304

$$305 \quad S^a(\tau, \mu) = \frac{\omega}{4\pi} F_s P(\tau, -\mu_0, \mu) \exp\left(\frac{-\tau}{\mu_0}\right) + \frac{\omega}{4\pi} F_s R(-\mu_0, m) P(\tau, +\mu_0, \mu) \exp\left(\frac{-(2\tau^a - \tau)}{\mu_0}\right)$$

307 (7)

308

309 where $R(-\mu_0, m)$ is the Fresnel reflectance of radiation and m is the ratio of the
 310 refractive indices of the lower to the upper medium. For the medium below the refractive
 311 interface, one must account for the Fresnel transmittance $T(-\mu_0, m)$ and modify the
 312 angle of beam travel in media b:

313

$$314 \quad S^b(\tau, \mu) = \frac{\omega}{4\pi} \frac{\mu_0}{\mu_{0n}} F_s T(-\mu_0, m) P(\tau, -\mu_0, \mu) \exp\left(\frac{-\tau^a}{\mu_0}\right) \exp\left(\frac{-(\tau - \tau^a)}{\mu_{0n}}\right)$$

315 (8)

315

316 where μ_{0n} is the cosine zenith angle of refracted beam incident at angle μ_0 above the
 317 refractive boundary, by Snell's law:

318

$$319 \quad \mu_{0n} = \sqrt{1 - (1 - \mu_0^2)/m^2}$$

320 (9)

320

321 For uniformly refractive media like snow on land, one can just set the refractive index m_{re}
 322 equal to 1 for every layer. In this case, the Fresnel reflectance $R(-\mu_0, m)$ is 0 in equation
 323 (7), the Fresnel transmittance $T(-\mu_0, m)$ is 1 in equation (8), and μ_{0n} equals to μ_0 : the
 324 two source terms $S^a(\tau, \mu)$ and $S^b(\tau, \mu)$ become the same and equal to the source term of
 325 homogenous media given in equation (2).

326

327 For two-stream approximations of this method, analytical solutions of upward and
 328 downward fluxes are coupled at each layer interface to generate 2N equations with 2N
 329 unknown coefficients for any N-layer stratified column. The solutions of two-stream
 330 algorithms and boundary conditions for homogenous media are well documented
 331 (Sections 8.4 and 8.10 of Thomas and Stamnes, 1999). Despite the extra source terms,
 332 these 2N equations can also be organized into a tridiagonal matrix similar to the method
 333 of Toon et al. (1989) used in SNICAR. Flexibility and speed therefore make this two-
 334 stream discrete-ordinate algorithm (hereafter, 2SD) a potentially good candidate for long-

335 | term Earth system modeling. In this work, we only apply 2SD to [the](#) snowpack and note
336 | that it can be applied to any uniformly or non-uniformly refractive media like snow on
337 | land or sea ice, with the Delta-transform implemented to fundamental optical variables
338 | (Equations 2 (a)-(c), Wiscombe and Warren, 1980).

339

340 2.4 16-stream DISORT

341 | Besides the mathematical technique, the accuracy and speed of radiative transfer
342 | algorithms depend on the number of angles used for flux estimation in the upward and
343 | downward hemispheres. SNICAR, dEdd-AD, and 2SD use one angle to represent upward
344 | flux and one angle to represent downward flux, hence they are named two-stream
345 | algorithm. Lee and Liou (2007) use two upward and two downward streams. Jin and
346 | Stamnes (1994) documented the solutions for any even number of streams. The
347 | computational efficiency of these models is lower than that of two-stream models while
348 | their accuracy is better. To quantify the accuracy of the three two-stream algorithms for
349 | snow shortwave simulations, we use the 16-stream DIScrete-Odinate Radiative Transfer
350 | model (DISORT) as the benchmark model (<http://llab.phy.stevens.edu/disort/>) (Stamnes
351 | et al., 1988).

352

353 3. Input for radiative transfer models

354 | In this work, we focus on the performance of two-stream algorithms for pure snow
355 | simulations. The inputs for these three models are the same: single-scattering properties
356 | (SSPs, i.e. single-scattering albedo ω , asymmetry factor g , extinction coefficient σ_{ext}) of
357 | snow determined by snow grain radius r , snow depth, solar zenith angle θ , solar incident
358 | flux, and the albedo of underlying ground (assuming Lambertian reflectance of 0.25 for
359 | all wavelengths). A Delta-transform is applied to fundamental input optical variables for
360 | all simulations (Equations 2 (a)-(c), Wiscombe and Warren, 1980).

361

362 | In snow, photon scattering occurs at the air-ice interface, and the absorption of photons
363 | occurs within the ice crystal. The most important factor that determines snow shortwave
364 | properties is the ratio of total surface area to total mass of snow grains, aka “the specific
365 | surface area” (e.g. Matzl and Schneebeli, 2006, 2010). The specific surface area (β) can
366 | be converted to a radiatively effective snow grain radius r :

367

$$368 \quad \beta = 3 / (r \rho_{ice}) \quad (10)$$

369

370 where ρ_{ice} is the density of pure ice, 917 kg m^{-3} . Assuming the grains are spherical, the
371 SSPs of snow can thus be computed using Mie theory (Wiscombe, 1980) and ice optical
372 constants (Warren and Brandt, 2008). In nature, snow grains are not spherical, and many
373 studies have been carried out to quantify the accuracy of such spherical representations
374 (Grenfell and Warren, 1999; Neshyba et al., 2003; Grenfell et al., 2005). In recent years,
375 more research has been done to evaluate the impact of grain shape on snow shortwave
376 properties (Dang et al., 2016; He et al., 2017, 2018ab), and they show that non-spherical
377 snow grain shapes mainly alter the asymmetry factor. Dang et al., (2016) also point out
378 that the solar properties of a snowpack consisting of non-spherical ice grains can be
379 mimicked by a snowpack consisting of spherical grains with a smaller grain size by
380 factors up to 2.4. In this work, we still assume the snow grains are spherical, and this
381 assumption does not qualitatively alter our evaluation of the radiative transfer algorithms.
382

383 The input SSPs of snow grains are computed using Mie theory at a fine spectral
384 resolution for a wide range of ice effective radius r from 10 to $3000 \mu\text{m}$ that covers the
385 possible range of grain radius for snow on Earth (Flanner et al., 2007). The same spectral
386 SSPs were also used to derive the band-averaged SSPs of snow used in SNICAR. Note
387 Briegleb and Light (2007) refer to SSPs as inherent optical properties.
388

389 4. Solar spectra used for the spectral integrations

390 In climate modeling, snow albedo computation at a fine spectral resolution is expensive
391 and unnecessary. Instead of computing spectrally resolved snow albedo, wider-band solar
392 properties are more practical. For example, CESM and E3SM aggregate the narrow
393 RRTMG bands used for the atmospheric radiative transfer simulation into visible (0.2 -
394 $0.7 \mu\text{m}$) and near-IR (0.7 - $5 \mu\text{m}$) bands. The land model and sea-ice model thus receive
395 visible and near-IR fluxes as the upper boundary condition, and return the corresponding
396 visible and near-IR albedos to atmosphere model. In practice, these bands are also
397 partitioned into direct and diffuse components. Therefore, a practical two-stream
398 algorithm should be able to simulate the direct visible, diffuse visible, direct near-IR and
399 diffuse near-IR albedos and absorptions of snow accurately.
400

401 The band albedo α is an irradiance-weighted average of the spectral albedo $\alpha(\lambda)$:

$$402 \alpha = \frac{\int_{\lambda_1}^{\lambda_2} \alpha(\lambda) F(\lambda) d\lambda}{\int_{\lambda_1}^{\lambda_2} F(\lambda) d\lambda} \quad (11)$$

403
404
405

Author 6/28/19 4:17 PM

Deleted: as shown in Figure 1

407 In this work, we use the spectral irradiance $F(\lambda)$ generated by the atmospheric DISORT-
408 based Shortwave Narrowband Model (SWNB2) (Zender et al., 1997; Zender, 1999) for
409 typical clear-sky and cloudy-sky conditions of mid-latitude winter as shown in Figure
410 [1\(a\)](#). The total clear-sky down-welling surface flux at different solar zenith angles are
411 also given in Figure [1\(b\)](#).

412
413

414 5. Model Evaluation

415 5.1 Spectral albedo and reflected solar flux

416 The spectral reflectance of pure deep snow computed using two-stream models and 16-
417 stream DISORT are shown in [Figure 2](#). The snow grain radius is $100 \mu\text{m}$ - a typical grain
418 size for fresh new snow. For clear sky with direct beam source (left column), all three
419 two-stream models show good accuracy at visible wavelengths ($0.3 - 0.7 \mu\text{m}$), and within
420 this band, the snow albedo is large and close to 1. As wavelength increases, the albedo
421 diminishes in the near-IR band. Two-stream models overestimate snow albedo at these
422 wavelengths, with maximum biases of 0.013 (SNICAR and dEdd-AD) and 0.023 (2SD)
423 within wavelength $1 - 1.7 \mu\text{m}$. For cloudy-sky cases with diffuse upper boundary
424 conditions, dEdd-AD reproduces the snow albedo at all wavelengths with the smallest
425 absolute error (< 0.005), SNICAR and 2SD both overestimate the snow albedo with
426 maximum biases > 0.04 between $1.1-1.4 \mu\text{m}$.

427

428 In both sky conditions, the errors of snow albedo are larger at near-IR wavelengths
429 ranging from $1.0-1.7 \mu\text{m}$, while the solar incident flux peaks at $0.5 \mu\text{m}$ then decrease as
430 wavelength increases. The largest error in reflected flux is within the $0.7-1.5 \mu\text{m}$ band for
431 SNICAR and 2SD, as shown in the 3rd row of [Figure 1](#), dEdd-AD overestimate the direct
432 snow albedo mostly at wavelengths larger than $1.5 \mu\text{m}$ where the error in reflected flux is
433 almost negligible.

434

435 5.2 Broadband albedo and reflected solar flux

436 Integrated over the visible and near-IR wavelengths, the error in band albedos computed
437 using two-stream models for different cases are shown in Figure 3-6.

438

439 Figure 3 shows the error in direct band albedo for fixed snow grain radius of $100 \mu\text{m}$ with
440 different snow depth and solar zenith angles. As introduced in Section 2, SNICAR and
441 dEdd-AD both use delta-Eddington method to compute the visible albedo. They
442 overestimate the visible albedo for solar zenith angles smaller than 50° by up to 0.005,

Author 6/28/19 4:17 PM

Deleted: 2

Author 6/28/19 4:17 PM

Deleted: 2

Author 6/28/19 4:20 PM

Deleted: Figure

Author 6/28/19 4:17 PM

Deleted: 1

Author 7/15/19 12:27 AM

Deleted: . t

Author 6/28/19 4:20 PM

Deleted: Figure

Author 6/28/19 4:17 PM

Deleted: 1

450 and underestimate it for solar zenith angles larger than 50° by up to -0.01 . 2SD produces
451 similar results for the visible band but at a larger solar zenith angle threshold of 75° . In
452 the near-IR band, SNICAR and 2SD overestimate the snow albedo for solar zenith angles
453 smaller than 70° , beyond this, the error in albedo increases by up to -0.1 as solar zenith
454 angle increases. dEdd-AD produces a similar error pattern with a smaller solar zenith
455 angle threshold at 60° . As snow ages, its average grain size increases. For typical old
456 melting snow of grain radius $1000\ \mu\text{m}$ (Figure 4), two-stream models produce similar
457 errors of direct albedo in all bands. For snow consisting of smaller grain size, two-stream
458 models produce larger errors for visible albedo. Integrating over the entire solar band, the
459 three two-stream models evaluated show similar error patterns for direct albedo.

460

461 For a fixed solar zenith angle of 60° , the error of direct albedo for different snow depth
462 and snow grain radii are shown in Figure 5. SNICAR and dEdd-AD underestimate the
463 visible albedo in most scenarios, while 2SD overestimates the visible albedo for a larger
464 range of grain radius and snow depth. All three two-stream models tend to overestimate
465 the near-IR albedo except for shallow snow with large grain radius; the error of 2SD is
466 one order of magnitude larger than that of SNICAR and dEdd-AD.

467

468 Figure 6 is similar to Figure 5, but shows the diffuse snow albedo. In the visible band,
469 SNICAR and dEdd-AD generate similar errors in that they both underestimate the albedo
470 as snow grain size increases and snow depth decreases. 2SD overestimates the albedo
471 with a maximum error of around 0.015 . In the near-IR, two-stream models tend to
472 overestimate snow albedo, while the magnitude of biases produced by SNICAR and 2SD
473 are one order larger than that of dEdd-AD with the maximum error of 0.035 generated by
474 SNICAR. As a result, the all-wave diffuse albedos computed using dEdd-AD are more
475 accurate than those computed using SNICAR and 2SD.

476

477 Figures 7, 8 and 9 show the errors in reflected shortwave flux caused by snow albedo
478 errors seen in Figures 3, 4, and 6. In general, two-stream models produce larger errors in
479 reflected direct near-IR flux (Figure 7 and 8), especially with the 2SD model: the
480 maximum overestimate of reflected near-IR flux is $6\text{-}8\ \text{Wm}^{-2}$ for deep melting snow with
481 solar zenith angle $< 30^\circ$. Errors in reflected direct visible flux are smaller (mostly within
482 $\pm 1\ \text{Wm}^{-2}$) for all models in most scenarios, and become larger (mostly within $\pm 3\ \text{Wm}^{-2}$) as
483 snow grain size increases to $1000\ \mu\text{m}$ if computed using 2SD. As shown in Figure 9, for
484 diffuse flux with solar zenith angle of 60° at TOA, SNICAR and dEdd-AD generate

485 small errors in reflected visible flux (mostly within $\pm 1 \text{ Wm}^{-2}$), while 2SD always
486 overestimates reflected visible flux by up to 5 Wm^{-2} . In the near-IR, SNICAR and 2SD
487 overestimate reflected flux by as much as $10\text{-}12 \text{ Wm}^{-2}$; the error in reflected near-IR flux
488 produced by dEdd-AD is much smaller, mostly within $\pm 1 \text{ Wm}^{-2}$.

489

490 In general, dEdd-AD produces the most accurate albedo and thus reflected flux for both
491 direct and diffuse components. SNICAR is similar to dEdd-AD for its accuracy of direct
492 albedo and flux, yet generates large error for the diffuse component. 2SD tends to
493 overestimate snow albedo and reflected flux in both direct and diffuse components and
494 shows the largest errors among three two-stream models. Although the differences
495 between algorithms are small, they can have a notable impact on snowpack melt. For
496 example, compared to dEdd-AD, SNICAR and 2SD overestimate the diffuse albedo by
497 ~ 0.015 for melting snow (Figure 6). In Greenland, the daily averaged downward diffuse
498 solar flux from May to September is 200 W/m^2 , and the averaged cloud cover fraction is
499 80% (Figure 6, Dang et al., 2017). In this case, SNICAR and 2SD overestimate the
500 reflected solar flux by 2.4 W/m^2 per day – the amount of energy otherwise enough to melt
501 10 cm of snow water equivalent from May to September. dEdd-AD also remediates
502 compensating spectral biases (where visible and Near-IR biases are of opposite signs)
503 present in the other schemes. Those spectral biases do not affect the broadband fluxes
504 like the diffuse biases, but they nevertheless degrade proper feedbacks between snow/ice
505 reflectance and heating.”

506

507 5.3 Band absorption of solar flux

508 Figure 10 shows absorption profiles of shortwave flux computed using the 16-stream
509 DISORT model, with errors in absorbed fractional solar flux computed using two-stream
510 models. The snowpack is 10-cm deep and is divided into 5 layers, each 2-cm thick. The
511 snow grain radius is set to $100 \mu\text{m}$. The figure shows fractional absorption for snow
512 layers 1-4 and the underlying ground with an albedo of 0.25.

513

514 As shown in the first column of Figure 10, for new snow with a radius of $100 \mu\text{m}$, most
515 solar absorption occurs in the top 2-cm snow layer, where roughly 10% and 15% of
516 diffuse and direct near-IR flux are absorbed and dominate the solar absorption within the
517 snowpack. In the second layer (2-4 cm), the absorption of solar flux is less than 1% and
518 gradually decreases within the interior layers. The underlying ground absorbs roughly 2%
519 of solar flux, mostly visible flux that penetrates the snowpack more efficiently. As snow

Author 6/28/19 10:06 PM

Deleted: These relatively small differences between algorithms may still yield large impact on snowpack.

Author 6/28/19 4:22 PM

Deleted: self-

524 ages and snow grain grows, photons penetrate deeper into the snowpack. For typical old
525 melting snow with a radius of 1000 μm , most solar absorption still occurs in the top 2-cm
526 snow layer, where roughly 20% and 14% of diffuse and direct near-IR flux are absorbed.
527 The second snow layer (2-4 cm) absorbs more near-IR solar flux by roughly 2%. More
528 photons can penetrate through the snowpack, and results in a high fractionally absorption
529 by the underlying ground, especially for the visible band. As snow depth increase, the
530 ground absorption will decrease for both snow radii.

531

532 Comparing to 16-stream DISORT, two-stream models underestimate the column solar
533 absorptions for new snow, and they overestimate them for old snow, especially for the
534 surface snow layer and the underground. Overall, dEdd-AD gives the most accurate
535 absorption profiles among the three two-stream models, especially for new snow.

536

537 **6. Correction for direct albedo for large solar zenith angles**

538

539 It has been pointed out in previous studies that the two-stream approximations become
540 poor as solar zenith angle approaches 90° (e.g. Wiscombe 1977, Warren 1982). As shown
541 in Figures 3 and 4, all three two-stream models underestimate the direct snow albedo for
542 large solar zenith angles. In the visible band, when the snow grain size is small, the error
543 in direct albedo is almost negligible (Figure 3); while as snow ages and snow grains
544 become larger, the error increases yet remains low if the snow is deep (Figure 4). In the
545 near-IR, the biases of albedo are also larger for larger snow grain radii. For a given snow
546 size, the magnitudes of such biases are almost independent of snow depth, and mainly
547 determined by the solar zenith angle. In general, the errors of all-wave direct albedo are
548 mostly contributed by the errors of near-IR albedo, especially for optically thick
549 snowpacks (i.e., semi-infinite), because the errors of direct albedo in the visible are
550 negligible compared with those in the near-IR. To improve the performance of two-
551 stream algorithms, we develop a parameterization that corrects the underestimated near-
552 IR snow albedo at large zenith angles.

553

554 Figure 11 shows the direct near-IR albedo and fractional absorption of 2-meter thick
555 snowpacks consisting of grains with radius 100 μm and 1000 μm , computed using two-
556 stream algorithms and 16-stream DISORT. For solar zenith angles $> 75^\circ$, two-stream
557 models underestimate snow albedo and overestimate solar absorption within the
558 snowpack, mostly in the top 2-cm of snow, and the differences among the three two-
559 stream models are small. In Section 5, we have shown that dEdd-AD produces the most

Author 6/28/19 4:23 PM

Deleted: (overestimate)

Author 6/28/19 4:23 PM

Deleted: (old)

562 | accurate snow albedo in general. With anticipated wide application of dEdd-AD, we
 563 | develop the following parameterization to adjust its low biases in computed near-IR
 564 | direct albedo.

566 | We define and compute R_{75+} as the ratio of direct semi-infinite near-IR albedo computed
 567 | using 16-stream DISORT ($\alpha_{16-DISORT}$) to that computed using dEdd-AD ($\alpha_{dEdd-AD}$), for
 568 | solar zenith angle $> 75^\circ$. This ratio is shown in Figure 11 (c) and can be parameterized as
 569 | a function of snow grain radius (r , unit in meter) and the cosine of incident solar zenith
 570 | angle (μ_0), as shown in Figure 11(c):

$$572 | R_{75+} = \frac{\alpha_{16-DISORT}}{\alpha_{dEdd-AD}} = c_1(\mu_0) \log_{10}(r) + c_0(\mu_0), \text{ for } \mu_0 < 0.26, \text{ i.e. } \theta_0 > 75^\circ \quad (12)$$

574 | where coefficients c_1 and c_0 are polynomial functions of μ_0 , as shown in Figure 11(d):

$$576 | c_1(\mu_0) = 1.304\mu_0^2 - 0.631\mu_0 + 0.086 \quad (13a)$$

$$577 | c_0(\mu_0) = 6.807\mu_0^2 - 3.338\mu_0 + 1.467 \quad (13b)$$

579 | Since two-stream models always underestimate snow albedo, R_{75+} always exceeds 1
 580 | (Figure 11c). We can then adjust the direct near-IR snow albedo ($\alpha_{dEdd-AD}$) and direct
 581 | near-IR solar absorption ($Fabs_{dEdd-AD}$) by snow computed using dEdd-AD with ratio
 582 | R_{75+} :

$$584 | \alpha_{dEdd-AD}^{adjust} = R_{75+} \alpha_{dEdd-AD} \quad (14a)$$

$$586 | Fabs_{dEdd-AD}^{adjust} = Fabs_{dEdd-AD} - (R_{75+} - 1) \alpha_{dEdd-AD} F_{nir} \quad (14b)$$

588 | where F_{nir} is the direct near-IR flux. This adjustment reduces the error of near-IR albedo
 589 | from negative 2-10% to within $\pm 0.5\%$ for solar zenith angles larger than 75° , and for
 590 | grain radii ranging from 30-1500 μm (Figure 12). Errors in broadband direct albedo are
 591 | therefore also reduced to < 0.01 . The direct near-IR flux absorbed by the snowpack
 592 | decreases after applying this adjustment.

593

Author 6/28/19 4:26 PM
 Deleted: .
 Author 6/28/19 4:26 PM
 Deleted: w

Author 6/28/19 10:11 PM
 Deleted: .

Author 6/28/19 10:12 PM
 Formatted: Font:Italic
 Author 6/28/19 4:50 PM
 Deleted:
 Author 6/28/19 10:12 PM
 Formatted: Font:Italic
 Author 6/28/19 4:52 PM
 Deleted:
 Author 6/28/19 10:12 PM
 Formatted: Not Superscript/ Subscript
 Author 6/28/19 9:38 PM
 Deleted: .
 Author 6/28/19 10:12 PM
 Formatted: Font:(Default) Times New Roman
 Author 6/28/19 10:12 PM
 Formatted: Font:(Default) Times New Roman
 Author 6/28/19 4:54 PM
 Formatted: Font:Not Italic

600 When the solar zenith angle exceeds 75° , our model adjusts the computed direct near-IR
601 albedo $\alpha_{\text{dEdd-AD}}$ by the ratio R_{75+} following equations 12-14a and reduces direct near-
602 IR absorption following equation 14b. If snow is divided into multiple layers, we assume
603 all decreased near-IR absorption (2^{nd} term on the right-hand side, equation 14b) is
604 confined within the top layer. This assumption is fairly accurate for the near-IR band,
605 since most absorption occurs at the surface of the snowpack (Figures 10 and 11). As
606 discussed previously, this parameterization is developed based on albedo computed using
607 $\alpha_{\text{dEdd-AD}}$. For models that do not use $\alpha_{\text{dEdd-AD}}$ but SNICAR and 2SD, the same
608 adjustment still applies given the small differences of near-IR direct albedo computed
609 using two-stream models (Figure 11). For models that adopt other radiative transfer
610 algorithms it is best for the developers to examine their model against a benchmark
611 model such as 16-stream DISORT or two-stream models discussed in this work before
612 applying this correction.

613

614 Although the errors of direct near-IR albedos are large for large solar zenith angles, the
615 absolute error in reflected shortwave flux is small (Figures 7 and 8) as the down-welling
616 solar flux reaches snowpack decreases as solar zenith angle increases (Figures 1(b)).
617 However, such small biases in flux can be important for high latitudes where the solar
618 zenith angle is large for many days in late winter and early spring.

619

620 7. Implementation of snow radiative transfer model in Earth system models

621

622 ESMs often use band-averaged SSPs of snow and aerosols for computational efficiency,
623 rather than using brute-force integration of spectral solar properties across each band (per
624 equation 11). Besides using different radiative transfer approximations, SNICAR and
625 $\alpha_{\text{dEdd-AD}}$ also adopt different methods to derive the band-averaged SSPs of snow for
626 different band schemes.

627

628 In SNICAR, snow solar properties are computed for 5 bands: one visible band (0.3 -
629 $0.7\mu\text{m}$), and four near-IR bands ($0.7 - 1\mu\text{m}$, $1 - 1.2\mu\text{m}$, $1.2 - 1.5\mu\text{m}$, and $1.5 - 5\mu\text{m}$).
630 The solar properties of four subdivided near-IR bands are combined by fixed ratios to
631 compute the direct/diffuse near-IR snow properties. These two sets of ratios are derived
632 offline based on the incident solar spectra of typical of mid-latitude winter for clear and
633 cloudy-sky conditions clear sky and cloudy sky, respectively (Figure 1(a)).

634

Author 6/28/19 4:58 PM

Deleted: It is important to note that

Author 6/28/19 4:58 PM

Deleted: al

Author 6/28/19 4:58 PM

Deleted: to

Author 6/28/19 5:02 PM

Deleted: remains

Author 6/28/19 4:59 PM

Deleted: broader

Author 6/28/19 4:59 PM

Deleted: narrower bands

641 The band-averaged SSPs of snow grains are computed following the Chandrasekhar
 642 Mean approach (Thomas and Stamnes, 1999, their Equation 9.27; Flanner et al., 2007).
 643 Specifically, spectral SSPs of snow grains are weighted into bands according to surface
 644 incident solar flux typical of mid-latitude winter for clear and cloudy sky conditions. In
 645 addition, the single-scattering albedo $\varpi(\lambda)$ of ice grains are also weighted by the
 646 hemispheric albedo $\alpha(\lambda)$ of an optically thick snowpack:

$$648 \quad \bar{\varpi}(\bar{\lambda}) = \frac{\int_{\lambda_1}^{\lambda_2} \varpi(\lambda) F(\lambda) \alpha(\lambda) d\lambda}{\int_{\lambda_1}^{\lambda_2} F(\lambda) \alpha(\lambda) d\lambda} \quad (15a)$$

$$649 \quad \bar{g}(\bar{\lambda}) = \frac{\int_{\lambda_1}^{\lambda_2} g(\lambda) F(\lambda) d\lambda}{\int_{\lambda_1}^{\lambda_2} F(\lambda) \alpha(\lambda) d\lambda} \quad (15b)$$

$$650 \quad \sigma_{ext}(\bar{\lambda}) = \frac{\int_{\lambda_1}^{\lambda_2} \sigma_{ext}(\lambda) F(\lambda) d\lambda}{\int_{\lambda_1}^{\lambda_2} F(\lambda) \alpha(\lambda) d\lambda} \quad (15c)$$

651
 652 Two sets of snow band-averaged SSPs are generated for all grain radii, suitable for direct
 653 and diffuse light, respectively. For each modeling step and band, SNICAR is called twice
 654 to compute the direct and diffuse snow solar properties.

655
 656 In dEdd-AD, the snow-covered sea ice properties are computed for 3 bands: one visible
 657 band (0.3 – 07 μm), and two near-IR bands (0.7 – 1.19 μm and 1.19 – 5 μm). The solar
 658 properties of these two near-IR bands are combined using ratios w_{nir1} and w_{nir2} for 0.7-1
 659 .19 μm and 1.19-5 μm , depending on the fraction of direct near-IR flux f_{nidr} :

$$661 \quad w_{nir1} = 0.67 + 0.11 * (1 - f_{nidr}) \quad (16a)$$

$$662 \quad w_{nir2} = 1 - w_{nir1} \quad (16b)$$

663
 664 The band SSPs of snow are derived by integrating the spectral SSPs and the spectral
 665 surface solar irradiance measured in the Arctic under mostly clear sky.

$$667 \quad \bar{\varpi}(\bar{\lambda}) = \int_{\lambda_1}^{\lambda_2} \varpi(\lambda) F(\lambda) d\lambda \quad (17a)$$

$$668 \quad \bar{g}(\bar{\lambda}) = \int_{\lambda_1}^{\lambda_2} g(\lambda) F(\lambda) d\lambda \quad (17b)$$

$$669 \quad \sigma_{ext}(\bar{\lambda}) = \int_{\lambda_1}^{\lambda_2} \sigma_{ext}(\lambda) F(\lambda) d\lambda \quad (17c)$$

670

671 In addition, the band-averaged single-scattering albedo $\varpi(\bar{\lambda})$ is also increased to $\varpi(\bar{\lambda})'$
672 until the band albedo computed using averaged SSPs matches the band albedo $\bar{\alpha}$ within
673 0.0001, where $\bar{\alpha}$ is:

674

$$675 \quad \bar{\alpha} = \int_{\lambda_1}^{\lambda_2} \alpha(\lambda) F(\lambda) d\lambda \quad (18)$$

676

677 dEdd-AD adopts this single set of band SSPs for both direct and diffuse computations. In
678 practice, the physical snow grain radius r is adjusted to a radiatively equivalent radius r_{eqv}
679 based on the fraction of direct flux in the near-IR band (f_{nidr}):

680

$$681 \quad r_{eqv} = (f_{nidr} + 0.8(1 - f_{nidr}))r \quad (19)$$

682

683 This r_{eqv} and the corresponding snow SSPs are then used in the radiative transfer
684 calculation. The computed direct and diffuse solar properties alone are less accurate,
685 while the combined all-sky broadband solar properties agree with SNICAR (Briegleb and
686 Light, 2007). As a result, for each modeling step and band, dEdd-AD radiative transfer
687 subroutine is called only once to compute both the direct and diffuse snow solar
688 properties simultaneously.

689

690 SNICAR and dEdd-AD also use different approaches to avoid numerical singularities. In
691 SNICAR, singularities occur when the denominator of term C_n^{\pm} in equation (3) equals to
692 zero (i.e., $\gamma^2 - 1/\mu_0^2 = 0$), where γ is determined by the approximation method and SSPs
693 of snow, and μ_0 is the cosine of the solar zenith angle (Equations 23 and 24, Toon et al.,
694 1989). When such a singularity is detected, SNICAR will shift μ_0 by + 0.02 or -0.02 to
695 obtain physically realistic radiative properties. In the dEdd-AD algorithm, singularities
696 arise only when $\mu_0 = 0$ (Equation 4). Therefore, in practice, for $\mu_0 < 0.01$, dEdd-AD
697 computes the sea-ice solar properties for $\mu_0 = 0.01$ to avoid unphysical results.

698

699 | **8. Towards a unified radiative transfer model for snow, sea ice, and land ice.**

700

701

Author 6/28/19 9:28 PM

Deleted:

Author 6/28/19 5:03 PM

Deleted: Discussion:

704 Based on the inter-comparison of three two-stream algorithms and their implementations
705 in ESMs, we formulated the following surface shortwave radiative transfer
706 recommendations for an accurate, fast, and consistent treatment for snow on land, land
707 ice, and sea ice in ESMs:

708

709 First, the two-stream delta-Eddington adding-doubling algorithm by Briegleb and Light
710 (2007) is unsurpassed as a radiative transfer core. The evaluation in Section 5 shows that
711 this algorithm produces the least error for snow albedo and solar absorption within
712 snowpack, especially under overcast skies. This algorithm applies well to both uniformly
713 refractive media such as snow on land, and to non-uniformly refractive media, such as
714 bare/snow-covered/ponded sea ice and bare/snow-covered land ice. Numerical
715 singularities occur only rarely (when $\mu_0 = 0$) and are easily avoided in model
716 implementations. Among the three two-stream algorithms discussed here, dEdd-AD is
717 also the most efficient one as it takes only $\sim 2/3$ of the time of SNICAR and 2SD to
718 compute solar properties of multi-layer snowpacks.

719

720 Second, any two-stream cryospheric radiative transfer model can incorporate the
721 parameterization described in Section 6 to adjust the low bias of direct near-IR snow
722 albedo and high bias of direct near-IR solar absorption in snow, for solar zenith angles
723 larger than 75° . These biases are persistent across all two-stream algorithms discussed in
724 this work, and should be corrected for snow-covered surfaces. Alternatively, adopting a
725 4-stream approximation would reduce or eliminate such biases, though at considerable
726 expense in computational efficiency.

727

728 | Third, in a cryospheric radiative transfer model, one should prefer physically based
729 parameterizations that are extensible and convergent (e.g., with increasing spectral
730 resolution) for the band-averaged SSPs and size distribution of snow. Although the
731 treatments used in SNICAR and dEdd-AD are both practical since they both reproduce
732 the narrowband solar properties with carefully derived band-averaged inputs as discussed
733 in Section 7, the snow treatment used in SNICAR is more physically based and
734 reproducible since it does not rely on subjective adjustment and empirical coefficients as
735 used in dEdd-AD. Specifically, the empirical adjustment to snow grain radius
736 implemented in dEdd-AD may not always produce compensating errors. For example, in
737 snow containing light-absorbing impurities such adjustment may also lead to biases in
738 aerosol absorption since the albedo reduction caused by light-absorbing particles does not
739 linearly depend on snow grain radius (Dang et al., 2015). For further model development

740 incorporating non-spherical snow grain shapes (Dang et al., 2016; He et al., 2018ab),
741 such adjustment on grain radius may fail as well. Moreover, SNICAR computes the snow
742 properties for four near-IR bands, which helps capture the spectral variation of albedo
743 (Figure 2) and therefore better represents near-IR solar properties. It is also worth noting
744 that unlike the radiative core of dEdd-AD, SNICAR is actively maintained with
745 numerous modifications and updates in the past decade (e.g. Flanner et al., 2012; He et
746 al., 2018b). Snow radiative treatments that follow SNICAR conventions for SSPs may
747 take advantage of these updates. Note that any radiative core that follows SNICAR SSP
748 conventions must be called twice to compute diffuse and direct solar properties,
749 respectively.

750

751 Fourth, a surface cryospheric radiative transfer model should flexibly accommodate
752 coupled simulations with distinct atmospheric and surface spectral grids. Both the 5-band
753 scheme used in SNICAR and the 3-band scheme used in dEdd-AD separate the visible
754 from near-IR spectrum at 0.7 μm . This boundary aligns with the Community
755 Atmospheric Model's original radiation bands (CAM; Neale et al., 2012), though not
756 with the widely used Rapid Radiative Transfer Model (RRTMG; Iacono et al., 2008)
757 which places 0.7 μm squarely in the middle of a spectral band. A mismatch in spectral
758 boundaries between atmospheric and surface radiative transfer schemes can require an
759 ESM to unphysically apportion energy from the straddled spectral bin when coupling
760 fluxes between surface and atmosphere. The spectral grids of surface and atmosphere
761 radiation need not be identical so long as the coarser grid shares spectral boundaries with
762 the finer grid. In practice maintaining a portable cryospheric radiative module such as
763 SNICAR requires a complex offline toolchain (Mie solver, spectral refractive indices for
764 air, water, ice, and aerosols, spectral solar insolation for clear and cloudy skies) to
765 compute, integrate, and rebin SSPs. Aligned spectral boundaries between surface and
766 atmospheric would simplify the development of efficient and accurate radiative transfer
767 for the coupled Earth system.

768

769 Last, it is important to note that, although we only examine the performance of the dEdd-
770 AD for pure snow in this work, this algorithm can be applied to the surface solar
771 calculation of all cryospheric components with or without light-absorbing particles
772 present. First, Briegleb and Light (2007) proved its accuracy for simulating ponded/bare
773 sea-ice solar properties against observations and a Monte Carlo radiation model. Second,
774 In CESM and E3SM, the radiative transfer simulation of snow on land ice is carried out
775 by SNICAR with prescribed land ice albedo. Adopting the dEdd-AD radiative core in

776 SNICAR will permit these ESMs to couple the snow and land ice as a non-uniformly
777 refractive column for more accurate solar computations since bare/snow-covered/ponded
778 land ice is physically similar to bare/snow-covered/ponded sea ice, and the latter is
779 already treated well by dEdd-AD radiative transfer core. Third, adding light-absorbing
780 particles in snow will not change our results qualitatively. Both dEdd-AD and SNICAR
781 simulate the impact of light-absorbing particles (black carbon and dust) on snow and/or
782 sea ice using self-consistent particle SSPs that follow the SNICAR convention (e.g.,
783 Flanner et al., 2007; Holland et al. 2012). These particles are assumed to be either
784 internally or externally mixed with snow crystals; the combined SSPs of mixtures (e.g.
785 Appendix A of Dang et al., 2015) are then used as the inputs for radiative transfer
786 calculation. The adoption of dEdd-AD radiative transfer algorithm in SNICAR, and the
787 implementation of SNICAR snow SSPs in dEdd-AD enables a consistent simulation of
788 the radiative effects of light-absorbing particles in the cryosphere across ESM
789 components.

790

791 In summary, this inter-comparison and evaluation has shown multiple ways that the solar
792 properties of cryospheric surfaces can be improved in the current generation of ESMs.
793 We have merged these findings into a hybrid model SNICAR-AD, which is primarily
794 composed of the radiative transfer scheme of dEdd-AD, 5-band snow/aerosol SSPs of
795 SNICAR, and the parameterization to correct for snow albedo biases when solar zenith
796 angle exceeds 75° . This hybrid model can be applied to snow on land, land ice, and sea
797 ice to produce consistent shortwave radiative properties for snow-covered surfaces across
798 the Earth system. With the evolving and further understanding of snow and aerosol
799 physics and chemistry, the adoption of this hybrid model will obviate the effort to modify
800 and maintain separate optical variable input files used for different model components.

801

802 SNICAR-AD is now implemented in both the sea-ice (MPAS-seaice) and land (ELM)
803 components of E3SM. More simulations and analyses are underway to examine its
804 impact on E3SM model performance and simulated climate. The results are however
805 beyond the scope of this work and will be thoroughly discussed in a future paper.

806

807 **9. Conclusions**

808 In this work, we aim to improve and unify the solar radiative transfer calculations for
809 snow on land and snow on sea ice in ESMs by evaluating the following two-stream
810 radiative transfer algorithms: the two-stream delta-Eddington adding-doubling algorithm
811 dEdd-AD implemented in sea-ice model Icepack/CICE/MPAS-seaice, the two-stream

812 delta-Eddington and two-stream delta-Hemispheric-Mean algorithms implemented in
813 snow model SNICAR, and a two-stream delta-Discrete-Ordinate algorithm. Among these
814 three models, the dEdd-AD produces the most accurate snow albedo and solar absorption
815 (Section 5). All two-stream models underestimate near-IR snow albedo and overestimate
816 near-IR absorption when solar zenith angles are larger than 75° , which can be adjusted by
817 a parameterization we developed (Section 6). We compared the implementations of
818 radiative transfer cores in SNICAR and dEdd-AD (Section 7) and recommended a
819 consistent and hybrid shortwave radiative model SNICAR-AD for snow-covered surfaces
820 across ESMs (Section 8). Improved treatment of surface cryospheric radiative properties
821 in the thermal infrared has recently been shown to remediate significant climate
822 simulation biases in Polar Regions (Huang et al., 2018). It is hoped that adoption of
823 improved and consistent treatments of solar radiative properties for snow-covered
824 surfaces as described in this study will further remediate simulation biases in snow-
825 covered regions.
826

827 **Data availability.** The data and models are available upon request to Cheng Dang
828 (cdang5@uci.edu). SNICAR and dEdd-AD radiative transfer core can be found at
829 <https://github.com/E3SM-Project/E3SM>.
830

831 **Competing interests.** The authors declare that they have no conflict of interest.
832

833 **Acknowledgments.** The authors thank Prof. Stephen G. Warren and Prof. Qiang Fu for
834 insightful discussions on radiative transfer algorithms. The authors thank Dr. Adrian
835 Turner for instructions on installing and running MPAS-seaice. The authors thank Dr.
836 David Bailey and one anonymous reviewer for their constructive comments that
837 improved our manuscript. This research is supported as part of the Energy Exascale Earth
838 System Model (E3SM) project, funded by the U.S. Department of Energy, Office of
839 Science, Office of Biological and Environmental Research, with funding number DE-
840 SC0012998.
841

842 **References**

- 843 Aoki, T., Kuchiki, K., Niwano, M., Kodama, Y., Hosaka, M. and Tanaka, T.: Physically
844 based snow albedo model for calculating broadband albedos and the solar heating
845 profile in snowpack for general circulation models. *Journal of Geophysical Research*,
846 116, D11114, <https://doi.org/10.1029/2010JD015507>, 2011.
- 847 Bøggild, C.E., Brandt, R.E., Brown, K.J. and Warren, S.G.: The ablation zone in
848 northeast Greenland: ice types, albedos and impurities. *Journal of Glaciology*, 56,
849 101-113, pp.101-113, <https://doi.org/10.3189/002214310791190776>, 2010.
- 850 Brandt, R.E., Warren, S.G., Worby, A.P. and Grenfell, T.C.: Surface albedo of the
851 Antarctic sea ice zone. *Journal of Climate*, 18(17), pp.3606-3622.
852 <https://doi.org/10.1175/JCLI3489.1> 2005.
- 853 Briegleb, P. and Light, B.: A Delta-Eddington multiple scattering parameterization for
854 solar radiation in the sea ice component of the community climate system model,
855 2007.
- 856 Dang, C. and Hegg, D.A.: Quantifying light absorption by organic carbon in Western
857 North American snow by serial chemical extractions. *Journal of Geophysical
858 Research*, 119(17), pp.10-247. <https://doi.org/10.1002/2014JD022156>, 2014.
- 859 Dang, C., Fu, Q. and Warren, S.G., 2016. Effect of snow grain shape on snow albedo.
860 *Journal of the Atmospheric Sciences*, 73(9), pp.3573-3583.
861 <https://doi.org/10.1175/JAS-D-15-0276.1>, 2016.
- 862 Dang, C., Brandt, R.E. and Warren, S.G.: Parameterizations for narrowband and
863 broadband albedo of pure snow and snow containing mineral dust and black carbon.
864 *Journal of Geophysical Research: Atmospheres*, 120(11), pp.5446-5468,
865 <https://doi.org/10.1002/2014JD022646>, 2015.
- 866 Dang, C., Warren, S.G., Fu, Q., Doherty, S.J., Sturm, M. and Su, J.: Measurements of
867 light-absorbing particles in snow across the Arctic, North America, and China:

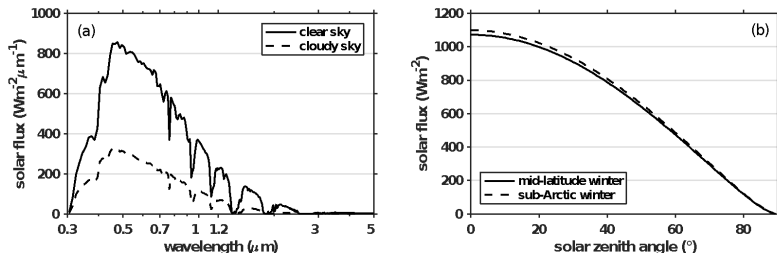
- 868 Effects on surface albedo. *Journal of Geophysical Research: Atmospheres*, 122(19),
869 pp.10-149. <https://doi.org/10.1002/2017JD027070>, 2017.
- 870 Doherty, S.J., Hegg, D.A., Johnson, J.E., Quinn, P.K., Schwarz, J.P., Dang, C. and
871 Warren, S.G.: Causes of variability in light absorption by particles in snow at sites in
872 Idaho and Utah. *Journal of Geophysical Research: Atmospheres*, 121(9), pp.4751-
873 4768. <https://doi.org/10.1002/2015JD024375>, 2016.
- 874 Doherty, S.J., Warren, S.G., Grenfell, T.C., Clarke, A.D. and Brandt, R.E.: Light-
875 absorbing impurities in Arctic snow. *Atmospheric Chemistry and Physics*. 10(23),
876 pp.11647-11680. <https://doi.org/10.5194/acp-10-11647-2010>, 2010.
- 877 Doherty, S.J., Dang, C., Hegg, D.A., Zhang, R. and Warren, S.G.: Black carbon and other
878 light-absorbing particles in snow of central North America. *Journal of Geophysical*
879 *Research: Atmospheres*, 119(22), pp.12-807, <https://doi.org/10.1002/2014JD022350>,
880 2014.
- 881 Flanner, M.G. and Zender, C.S.: Snowpack radiative heating: Influence on Tibetan
882 Plateau climate. *Geophysical Research Letters*, 32(6).
883 <https://doi.org/10.1029/2004GL022076>, 2005.
- 884 Flanner, M.G., Zender, C.S., Randerson, J.T. and Rasch, P.J.: Present-day climate forcing
885 and response from black carbon in snow. *Journal of Geophysical Research:*
886 *Atmospheres*, 112(D11). <https://doi.org/10.1029/2006JD008003>, 2007.
- 887 Flanner, M.G., Liu, X., Zhou, C., Penner, J.E. and Jiao, C.: Enhanced solar energy
888 absorption by internally-mixed black carbon in snow grains. *Atmospheric Chemistry*
889 *and Physics*, 12(10), pp.4699-4721. <https://doi.org/10.5194/acp-12-4699-2012>, 2012.
- 890 Gardner, A.S. and Sharp, M.J.: A review of snow and ice albedo and the development of
891 a new physically based broadband albedo parameterization. *Journal of Geophysical*
892 *Research: Earth Surface*, 115(F1). <https://doi.org/10.1029/2009JF001444>, 2010.
- 893 Grenfell, T.C., Neshyba, S.P. and Warren, S.G.: Representation of a nonspherical ice
894 particle by a collection of independent spheres for scattering and absorption of
895 radiation: 3. Hollow columns and plates. *Journal of Geophysical Research:*
896 *Atmospheres*, 110(D17). <https://doi.org/10.1029/2005JD005811>, 2005.
- 897 He, C., Liou, K.N., Takano, Y., Yang, P., Qi, L. and Chen, F.: Impact of grain shape and
898 multiple black carbon internal mixing on snow albedo: Parameterization and radiative
899 effect analysis. *Journal of Geophysical Research: Atmospheres*, 123(2), pp.1253-
900 1268. <https://doi.org/10.1002/2017JD027752>, 2018a.
- 901 He, C., Flanner, M.G., Chen, F., Barlage, M., Liou, K.N., Kang, S., Ming, J. and Qian,
902 Y.: Black carbon-induced snow albedo reduction over the Tibetan Plateau:
903 uncertainties from snow grain shape and aerosol–snow mixing state based on an
904 updated SNICAR model. *Atmospheric Chemistry and Physics*, 18, pp.11507-11527.
905 <https://doi.org/10.5194/acp-18-11507-2018>, 2018b.
- 906 He, C., Takano, Y., Liou, K.N., Yang, P., Li, Q. and Chen, F.: Impact of Snow Grain
907 Shape and Black Carbon–Snow Internal Mixing on Snow Optical Properties:
908 Parameterizations for Climate Models. *Journal of Climate*, 30(24), pp.10019-10036.
909 <https://doi.org/10.1175/JCLI-D-17-0300.1>, 2017.

- 910 Holland, M.M., Bailey, D.A., Briegleb, B.P., Light, B. and Hunke, E.: Improved sea ice
911 shortwave radiation physics in CCSM4: The impact of melt ponds and aerosols on
912 Arctic sea ice. *Journal of Climate*, 25(5), pp.1413-1430. [https://doi.org/10.1175/JCLI-
D-11-00078.1](https://doi.org/10.1175/JCLI-
913 D-11-00078.1), 2012.
- 914 Huang, X., Chen, X., Flanner, M., Yang, P., Feldman, D. and Kuo, C.: Improved
915 representation of surface spectral emissivity in a global climate model and its impact
916 on simulated climate. *Journal of Climate*, 31(9), pp.3711-3727.
917 <https://doi.org/10.1175/JCLI-D-17-0125.1>, 2018.
- 918 Hunke, E. C., Lipscomb, W. H., Turner, A. K., Jeffery, N., and Elliott, S.: CICE: the Los
919 Alamos Sea Ice Model Documentation and Software User's Manual Version 4.1 LA-
920 CC-06-012. T-3 Fluid Dynamics Group, Los Alamos National Laboratory 675. 2010.
- 921 Iacono, M.J., Delamere, J.S., Mlawer, E.J., Shephard, M.W., Clough, S.A. and Collins,
922 W.D.: Radiative forcing by long-lived greenhouse gases: Calculations with the AER
923 radiative transfer models. *Journal of Geophysical Research: Atmospheres*, 113(D13),
924 <https://doi.org/10.1029/2008JD009944>, 2008.
- 925 Jin, Z. and Stamnes, K.: Radiative transfer in nonuniformly refracting layered media:
926 atmosphere-ocean system. *Applied Optics*, 33(3), pp.431-442.
927 <https://doi.org/10.1364/AO.33.000431>, 1994.
- 928 Kuipers Munneke, P., Van den Broeke, M.R., Lenaerts, J.T.M., Flanner, M.G., Gardner,
929 A.S. and Van de Berg, W.J.: A new albedo parameterization for use in climate
930 models over the Antarctic ice sheet. *Journal of Geophysical Research: Atmospheres*,
931 116(D5). <https://doi.org/10.1029/2010JD015113>, 2011.
- 932 Lee, W.L. and Liou, K.N.: A coupled atmosphere-ocean radiative transfer system using
933 the analytic four-stream approximation. *Journal of the Atmospheric Sciences*, 64(10),
934 pp.3681-3694. <https://doi.org/10.1175/JAS4004.1>, 2007.
- 935 Liang, S., Fang, H., Chen, M., Shuey, C.J., Walthall, C., Daughtry, C., Morisette, J.,
936 Schaaf, C. and Strahler, A.: Validating MODIS land surface reflectance and albedo
937 products: Methods and preliminary results. *Remote sensing of environment*, 83(1-2),
938 pp.149-162. [https://doi.org/10.1016/S0034-4257\(02\)00092-5](https://doi.org/10.1016/S0034-4257(02)00092-5), 2002.
- 939 Light, B., Grenfell, T. C. and Perovich, D.K.: Transmission and absorption of solar
940 radiation by Arctic sea ice during the melt season. *Journal of Geophysical Research:*
941 *Oceans* 113, no. C3, <https://doi.org/10.1029/2006JC003977>, 2008.
- 942 Light, B., Perovich, D.K., Webster M.A., Polashenski, C., and Dadic, R.: Optical
943 properties of melting first-year Arctic sea ice. *Journal of Geophysical Research:*
944 *Oceans* 120, no. 11: 7657-7675, <https://doi.org/10.1002/2015JC011163>, 2015.
- 945 Marshall, S. and Oglesby, R.J.: An improved snow hydrology for GCMs. Part 1: Snow
946 cover fraction, albedo, grain size, and age. *Climate Dynamics*, 10(1-2), pp.21-37.
947 <https://doi.org/10.1007/BF00210334>, 1994.
- 948 Marshall, S.E.: A Physical Parameterization of Snow Albedo for Use in Climate Models,
949 NCAR Cooperative Thesis 123, National Center for Atmospheric Research,
950 Boulder, CO, 175 pp. 1989.

- 951 Matzl, M. and Schneebeli, M.: Measuring specific surface area of snow by near-infrared
952 photography. *Journal of Glaciology*, 52(179), pp.558-564.
953 <https://doi.org/10.3189/172756506781828412>, 2006.
- 954 Matzl, M. and Schneebeli, M.: Stereological measurement of the specific surface area of
955 seasonal snow types: Comparison to other methods, and implications for mm-scale
956 vertical profiling. *Cold Regions Science and Technology*, 64(1), pp.1-8.
957 <https://doi.org/10.1016/j.coldregions.2010.06.006>, 2010.
- 958 Meador, W.E. and Weaver, W.R.: Two-stream approximations to radiative transfer in
959 planetary atmospheres: A unified description of existing methods and a new
960 improvement. *Journal of the Atmospheric Sciences*, 37(3), pp.630-643.
961 [https://doi.org/10.1175/1520-0469\(1980\)037<0630:TSATRT>2.0.CO;2](https://doi.org/10.1175/1520-0469(1980)037<0630:TSATRT>2.0.CO;2), 1980.
- 962 Mlawer, E.J. and Clough, S.A.: On the extension of rapid radiative transfer model to the
963 shortwave region. In *Proceedings of the 6th Atmospheric Radiation Measurement*
964 *(ARM) Science Team Meeting, US Department of Energy, CONF-9603149*, 223–
965 226. 1997.
- 966 Neale, Richard B., Chen, C.-C., Gettelman, A., Lauritzen, P. H., Park, S., Williamson, D.
967 L., Conley, A. J., Garcia, R., Kinnison, D., Lamarque, J. F., and Marsh, D.:
968 Description of the NCAR community atmosphere model (CAM 5.0). NCAR Tech.
969 Note NCAR/TN-486+ STR 1, no. 1: 1-12. 2010.
- 970 Neshyba, S.P., Grenfell, T.C. and Warren, S.G.: Representation of a nonspherical ice
971 particle by a collection of independent spheres for scattering and absorption of
972 radiation: 2. Hexagonal columns and plates. *Journal of Geophysical Research:*
973 *Atmospheres*, 108(D15). <https://doi.org/10.1029/2002JD003302>, 2003.
- 974 Perovich, D. K.: The optical properties of sea ice (No. MONO-96-1). COLD REGIONS
975 RESEARCH AND ENGINEERING LAB HANOVER NH. 1996.
- 976 Stamnes, K., Tsay, S.C., Wiscombe, W. and Jayaweera, K.: Numerically stable algorithm
977 for discrete-ordinate-method radiative transfer in multiple scattering and emitting
978 layered media. *Applied optics*, 27(12), pp.2502-2509.
979 <https://doi.org/10.1364/AO.27.002502>, 1988.
- 980 Thomas, G.E. and K. Stamnes (1999), *Radiative transfer in the atmosphere and ocean*.
981 Cambridge University Press.
- 982 Toon, O. B., McKay, C. P., Ackerman, T. P., and Santhanam, K.: Rapid calculation of
983 radiative heating rates and photodissociation rates in inhomogeneous multiple
984 scattering atmospheres, *J. Geophys. Res.*, 94(D13), 16,287–16,301.
985 <https://doi.org/10.1029/JD094iD13p16287>, 1989.
- 986 Turner, A.K., Lipscomb, W.H., Hunke, E.C., Jacobsen, D.W., Jeffery, N., Ringler, T.D.
987 and Wolfe, J.D.: MPAS-Seaice: a new variable resolution sea-ice model. *J. Adv.*
988 *Model Earth Sy.*, in preparation., 2018.
- 989 Wang, X., Doherty, S.J. and Huang, J.: Black carbon and other light-absorbing
990 impurities in snow across Northern China. *Journal of Geophysical Research:*
991 *Atmospheres*, 118(3), pp.1471-1492. <https://doi.org/10.1029/2012JD018291>, 2013.

- 992 Warren, S. G.: Optical properties of snow. *Reviews of Geophysics* 20, no. 1: 67-89.
993 <https://doi.org/10.1029/RG020i001p00067,1982>.
- 994 Warren, S.G. and Wiscombe, W.J.: A model for the spectral albedo of snow. II: Snow
995 containing atmospheric aerosols. *Journal of the Atmospheric Sciences*, 37(12),
996 pp.2734-2745.[https://doi.org/10.1175/1520-](https://doi.org/10.1175/1520-0469(1980)037<2734:AMFTSA>2.0.CO;2,1980)
997 [0469\(1980\)037<2734:AMFTSA>2.0.CO;2, 1980](https://doi.org/10.1175/1520-0469(1980)037<2734:AMFTSA>2.0.CO;2,1980)
- 998 Warren, S.G. and Brandt, R.E.: Optical constants of ice from the ultraviolet to the
999 microwave: A revised compilation. *Journal of Geophysical Research: Atmospheres*,
1000 113(D14). [https://doi.org/10.1029/2007JD009744, 2008](https://doi.org/10.1029/2007JD009744,2008).
- 1001 Warren, S.G. and Wiscombe, W.J.: Dirty snow after nuclear war. *Nature*, 313(6002),
1002 p.467. [https://doi.org/10.1038/313467a0, 1985](https://doi.org/10.1038/313467a0,1985).
- 1003 Wiscombe, W. J.: The delta-Eddington approximation for a vertically inhomogeneous
1004 atmosphere, NCAR Tech. Note TN-140_STR [NTIS P6270618]. 1977.
- 1005 Wiscombe, W.J.: Improved Mie scattering algorithms. *Applied optics*, 19(9), pp.1505-
1006 1509. <https://doi.org/10.1364/AO.19.001505,1980>.
- 1007 Wiscombe, W.J. and Warren, S.G.: A model for the spectral albedo of snow. I: Pure
1008 snow. *Journal of the Atmospheric Sciences*, 37(12), pp.2712-2733.
1009 [https://doi.org/10.1175/1520-0469\(1980\)037<2712:AMFTSA>2.0.CO;2, 1980](https://doi.org/10.1175/1520-0469(1980)037<2712:AMFTSA>2.0.CO;2,1980).
- 1010 Zender, C.S.: Global climatology of abundance and solar absorption of oxygen collision
1011 complexes. *Journal of Geophysical Research: Atmospheres*, 104(D20), pp.24471-
1012 24484. [https://doi.org/10.1029/1999JD900797, 1999](https://doi.org/10.1029/1999JD900797,1999).
- 1013 Zender, C.S., Bush, B., Pope, S.K., Bucholtz, A., Collins, W.D., Kiehl, J.T., Valero, F.P.
1014 and Vitko Jr, J.: Atmospheric absorption during the atmospheric radiation
1015 measurement (ARM) enhanced shortwave experiment (ARESE). *Journal of*
1016 *Geophysical Research: Atmospheres*, 102(D25), pp.29901-29915.
1017 [https://doi.org/10.1029/97JD01781, 1997](https://doi.org/10.1029/97JD01781,1997).
- 1018

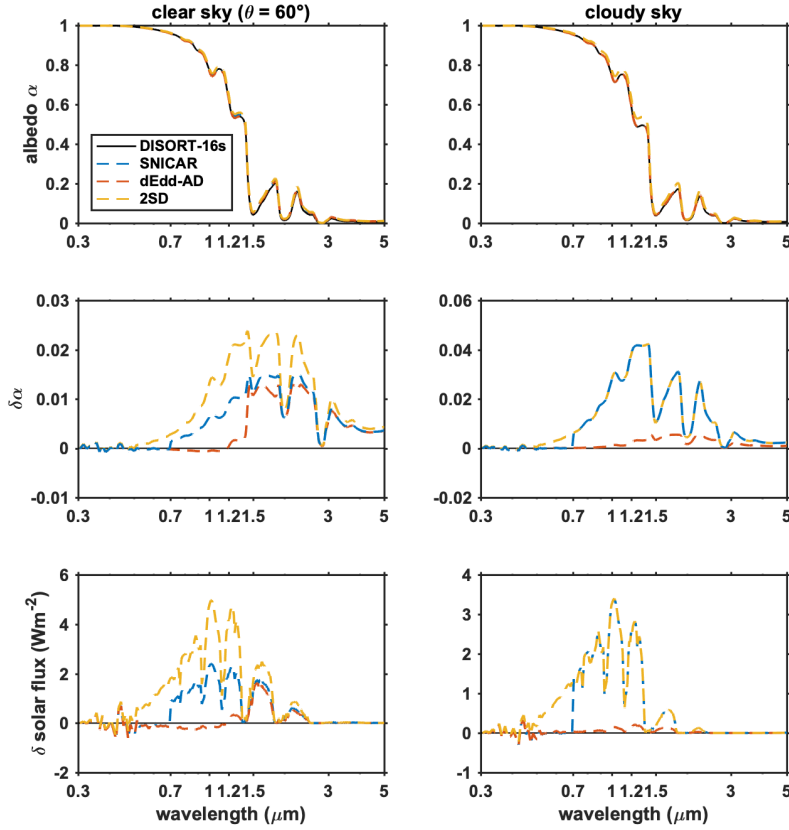
1019 | **Figure 1.** Spectral and total down-welling solar flux at surface computed using SWNB2
1020 for (a) standard clear-sky and cloudy-sky atmospheric profiles of mid-latitude winter
1021 assuming solar zenith angle is 60° at the top of the atmosphere, and for (b) standard clear
1022 sky profiles of mid-latitude and sub-Arctic winter with different incident solar zenith
1023 angles.
1024
1025



1026
1027
1028 |

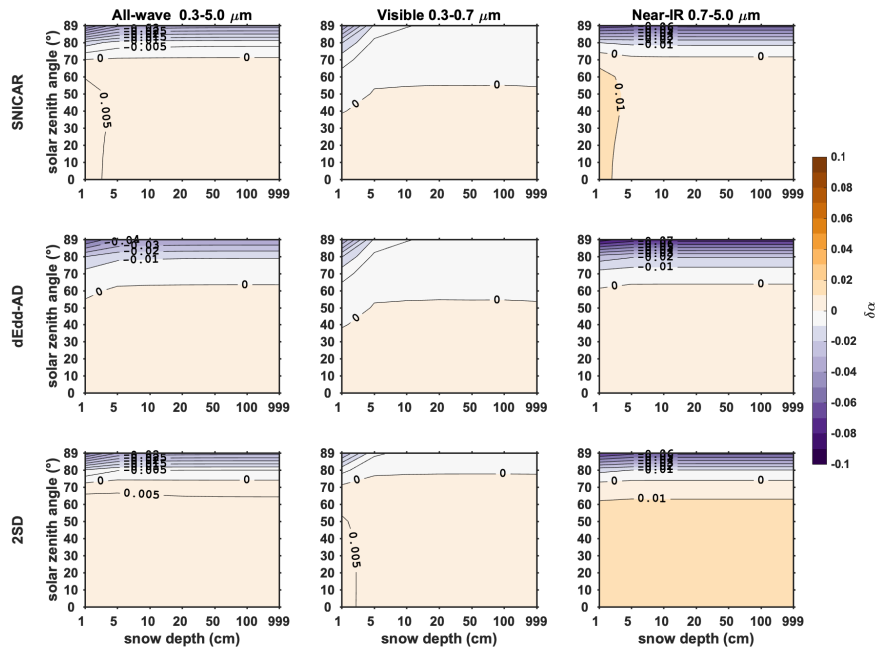
1029
1030
1031
1032
1033
1034
1035

Figure 2. The spectral albedo of pure snow computed using 16-stream DISORT, SNICAR, dEdd-AD, and 2SD models, for clear-sky (direct beam at solar zenith angle 60°) and cloudy-sky conditions in the left and right panels, respectively. The top panels show spectral albedo. The middle panels show the difference ($\delta\alpha = \alpha_s - \alpha_{16s}$) in spectral albedos computed using the two-stream model (α_s) and 16-stream DISORT (α_{16s}). The bottom panels show the difference of reflected spectral flux given $\delta\alpha$. The snowpack is set to semi-infinite deep with grain radius of $100 \mu\text{m}$.



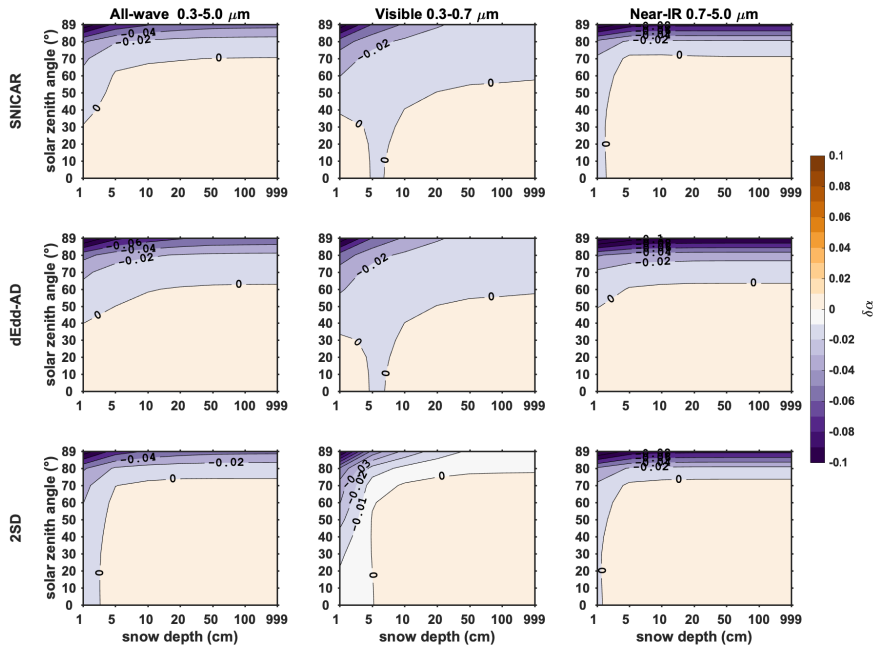
1036
1037
1038

1039 Figure 3. The difference in direct snow albedo ($\delta\alpha = \alpha_s - \alpha_{16}$) computed using two-stream
 1040 models (α_s) and using 16-stream DISORT model (α_{16}), for various snow depths and solar
 1041 zenith angles, with snow grain radius of $100 \mu\text{m}$. From the top to the bottom rows are
 1042 results of two-stream models SNICAR, dEdd-AD, and 2SD. From the left to the right
 1043 columns are albedo differences of all-wave, visible, near-IR bands.



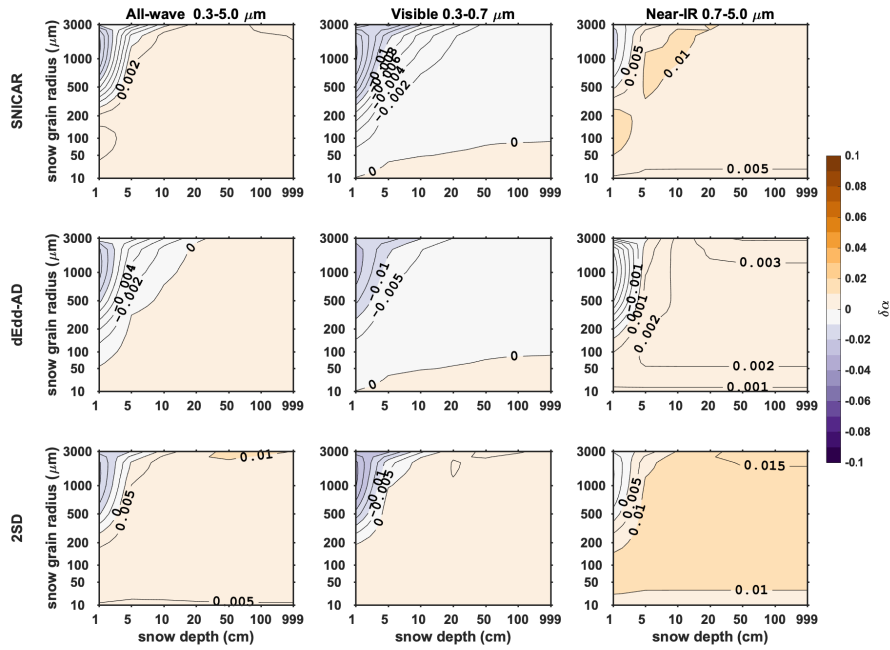
1044
 1045
 1046

1047 Figure 4. The difference in direct snow albedo ($\delta\alpha = \alpha_e - \alpha_{16}$) computed using two-stream
 1048 models (α_e) and using 16-stream DISORT model (α_{16}), for various snow depths and solar
 1049 zenith angles, with snow grain radius of 1000 μm .
 1050



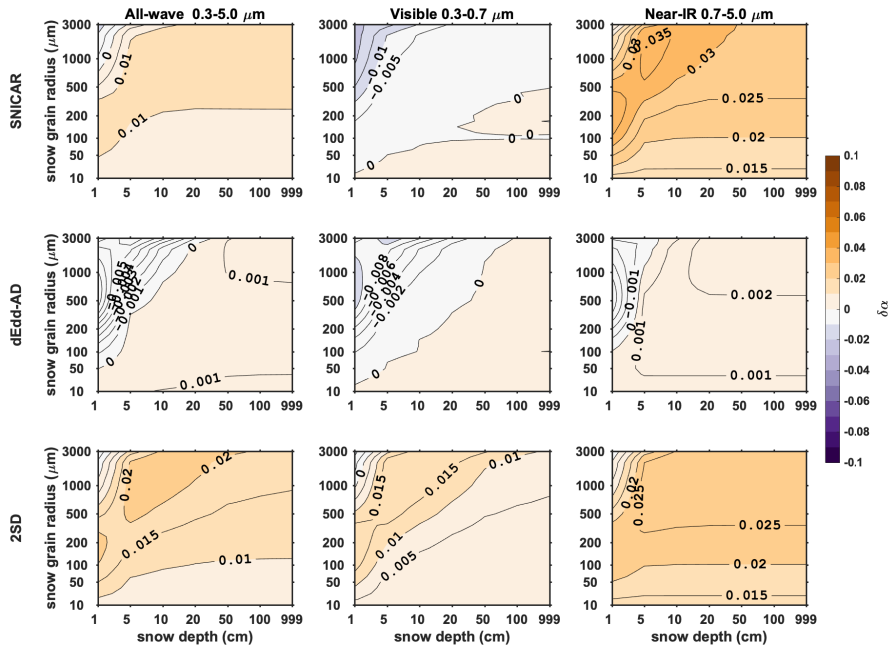
1051
 1052
 1053

1054 Figure 5. The difference in direct snow albedo ($\delta\alpha = \alpha_s - \alpha_{16}$) computed using two-stream
 1055 models (α_s) and using 16-stream DISORT model (α_{16}), for various snow depths and snow
 1056 grain radii, with solar zenith angle of 60° .
 1057



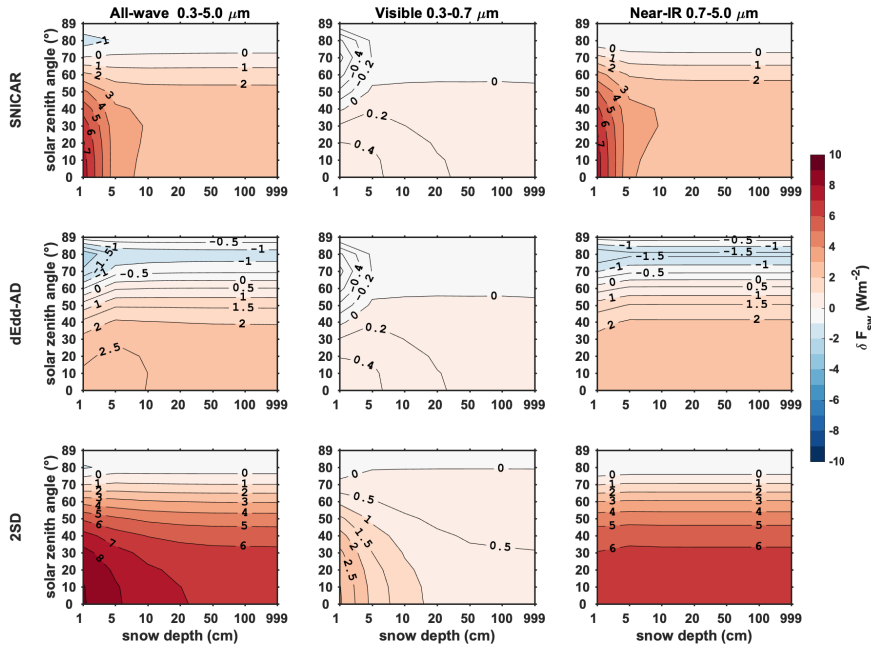
1058
 1059

1060 Figure 6. The difference in diffuse snow albedo ($\delta\alpha = \alpha_d - \alpha_{d,s}$) computed using two-
 1061 stream models (α_d) and using 16-stream DISORT model ($\alpha_{d,s}$), for various snow depths
 1062 and snow grain radii, with solar zenith angle of 60° at the top of the atmosphere.
 1063



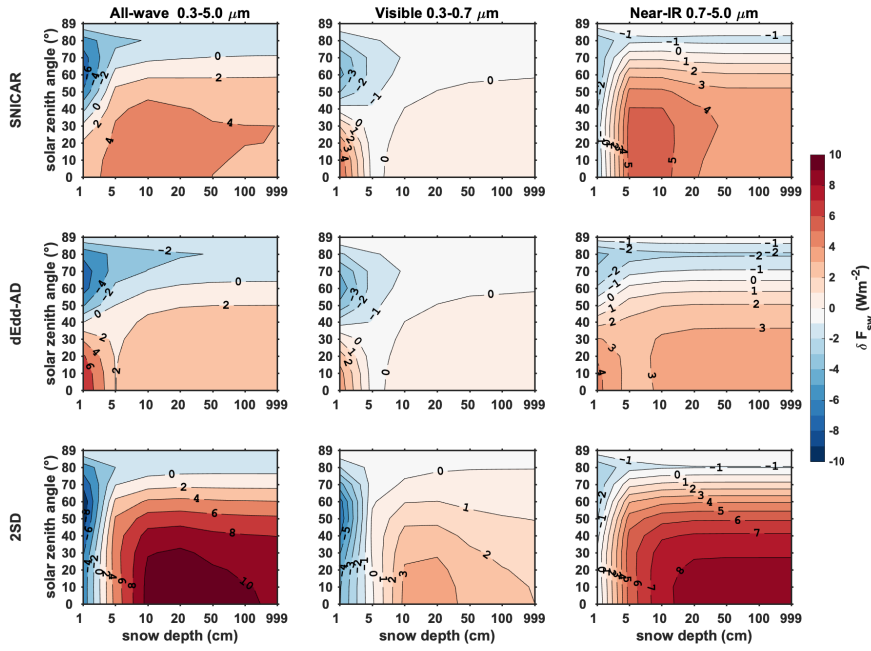
1064

1065 Figure 7. Error in reflected direct solar flux given albedo errors shown in Figure 3.



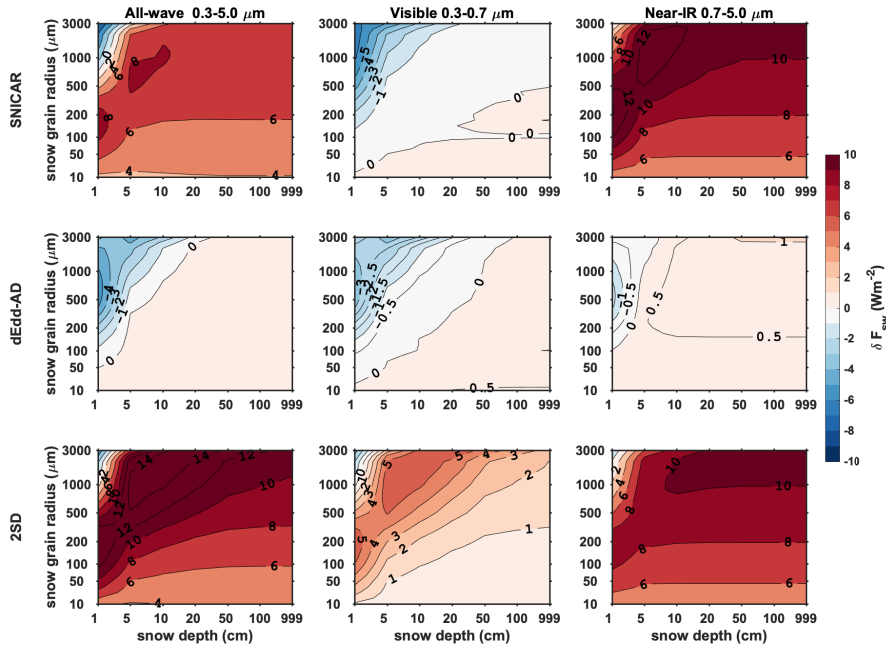
1066
1067

1068 Figure 8. Error in reflected direct solar flux given albedo errors shown in Figure 4.



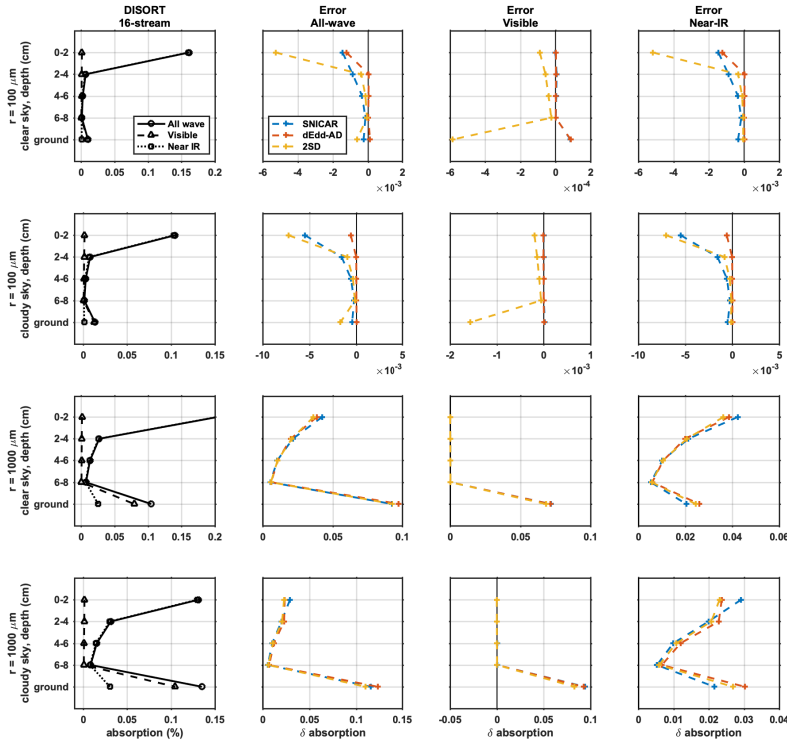
1069
1070
1071

1072 Figure 9. Error in reflected diffuse solar flux given albedo errors shown in Figure 6.



1073
1074
1075

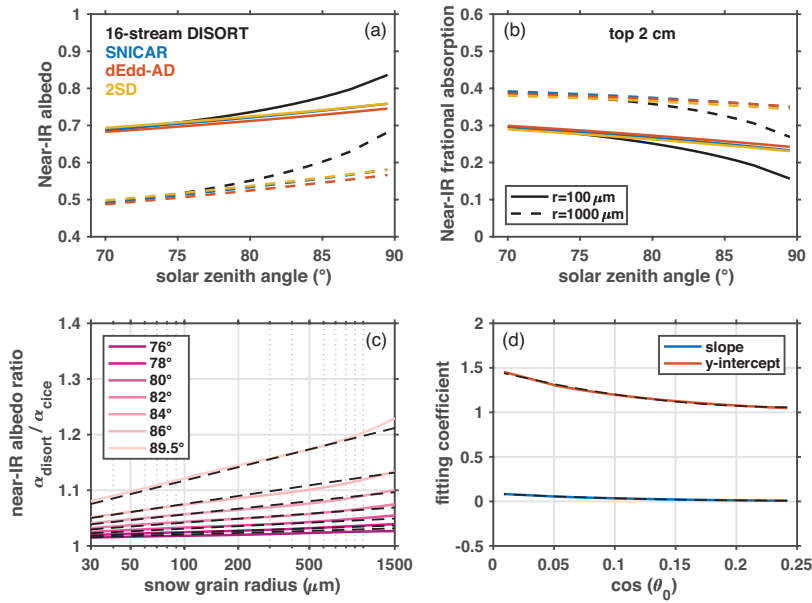
1076 Figure 10. Comparison of light-absorption profiles derived from two-stream models and
 1077 16-stream DISORT. The left-most column shows fractional band absorptions computed
 1078 using 16-stream DISORT. The right three panels show the errors of all-wave, visible, and
 1079 near-IR fractional absorptions calculated using two-stream models. The top and bottom
 1080 panels are for clear-sky and cloudy-sky conditions (solar zenith angle of 60°),
 1081 respectively. The snowpack is 10 cm deep and is divided evenly into five 2-cm thick
 1082 layers, for new snow ($r = 100 \mu\text{m}$) and old snow ($r = 1000 \mu\text{m}$). The layers 1-4 represent
 1083 the top four snow layers (top 8 cm), and layer 5 represents underlying ground with albedo
 1084 of 0.25.



1085
 1086

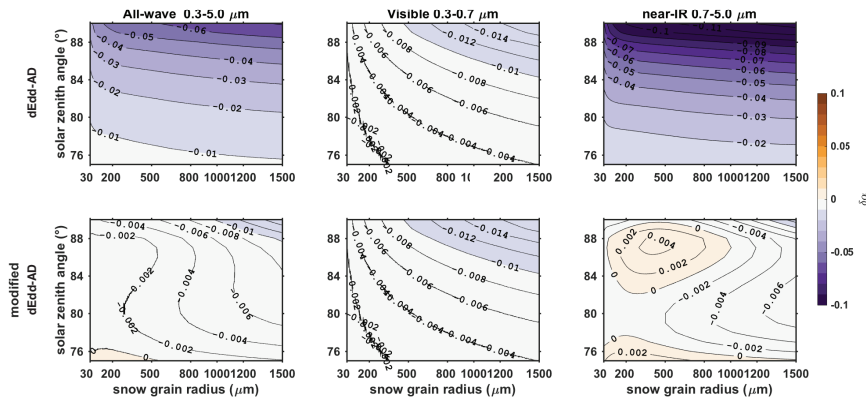
1087
1088
1089
1090
1091
1092
1093
1094

Figure 11. (a) Direct near-IR snow albedo and (b) near-IR fractional absorption by top 2-cm snow of a 2-m thick snowpack, for solar zenith angles larger than 70° and snow grain radii of $100\ \mu\text{m}$ and $1000\ \mu\text{m}$. (c) The ratios of near-IR albedo computed using CICE to that computed using 16-stream DISORT for different solar zenith angles. These ratios are parameterized as linear functions of the logarithmic of snow grain radius. The slopes and y-intercepts are shown in (d). The black dashed curves in figures (c) and (d) are fitting values computed using parameterization discussed in Section 5.



1095
1096
1097
1098

1099 Figure 12. Error in semi-infinite snow albedo computed using dEdd-AD before (top row)
 1100 and after (bottom row) incorporating corrections for near-IR albedo, for different solar
 1101 zenith angles and snow grain radii.
 1102



1103
 1104
 1105
 1106

1107 Table 1. Acronyms used in this paper and their references.
 1108
 1109

ESM/ESMs	Earth System Models	
E3SM	Energy Exscale Earth System Model	Global climate model, previously know as ACME, https://e3sm.org/
CESM	Community Earth System Model	Global climate model, http://www.cesm.ucar.edu/
CCSM	Community Climate System Model	Global climate model, http://www.cesm.ucar.edu/models/ccsm4.0/
RACMO	Regional Atmospheric Climate Model	Regional climate model, https://www.projects.science.uu.nl/iceclimate/models/racmo.php
CAM	Community Atmospheric Model	Atmospheric model, Neale et al., 2012
ELM	E3SM land model	Land component of E3SM, https://e3sm.org/model/e3sm-model-description/v1-description/
CLM	Community land model	Land component of CESM, http://www.cesm.ucar.edu/models/clm/
MPAS-seaice	Model for Prediction Across Scales Sea Ice	Sea-ice component of E3SM, Turner et al., 2018
CICE	Los Almos Sea Ice Model	Sea-ice component of CESM, Hunke et al., 2010
RRTM	Rapid Radiative Transfer Model	Standalone column radiative transfer model, Mlawer and Clough, 1997, http://rtweb.aer.com/rrtm_frame.html
RRTMG	Rapid Radiative Transfer Model for GCM components	Modified RRTM for GCM application, Iacono et al., 2008, http://rtweb.aer.com/rrtm_frame.html
DISORT	DIScrete-Odinate Radiative Transfer model	Standalone column radiative transfer model, http://llab.phy.stevens.edu/disort/ , Stamnes et al., 1988
SWNB2	Shortwave Narrowband Model	Standalone column radiative transfer model, Zender et al., 1997; Zender, 1999
SNICAR	SNow ICe and Aerosol Radiative module	Snow module used in ELM and CLM, Flanner and Zender, 2005; Toon et al., 1989

Author 6/28/19 5:08 PM

Deleted: model

Author 6/28/19 5:08 PM

Deleted: model

Author 6/28/19 5:08 PM

Deleted: model

Author 6/28/19 5:08 PM

Deleted: model

dEdd-AD	Two-stream delta-Eddington Adding-Doubling radiative transfer algorithm	Sea-ice radiative transfer core in MPAS-seaice and CICE, Briegleb and Light, 2007
2SD	Two-Stream Discrete ordinate radiative transfer algorithm	Radiative transfer algorithm tested in this work, Jin and Stamnes, 1994
SNICAR-AD	SNICAR – Adding Doubling	Hybrid snow/sea-ice radiative transfer model, Section 8
SSP/SSPs	Single-Scattering Properties	Single-scattering albedo ϖ , asymmetry factor g , extinction coefficient σ_{ext}
near-IR	Near Infrared band	Wavelengths of 0.7 - 5 μm

1114
1115

1116
 1117
 1118
 1119
 1120

Table 2. Two-stream radiative transfer algorithms evaluated in this work, including algorithms that are currently implemented in Earth System Model CESM and E3SM.

ESM Component	Land	Sea Ice	
Model	SNICAR	dEdd-AD	2SD
Radiative transfer approximation	two-stream δ -Eddington (visible) δ -Hemispheric-mean (near-IR)	two-stream δ -Eddington	two-stream δ -Discrete-ordinate
Treatment for multi-layered media	matrix inversion	adding-doubling	matrix inversion
Fresnel reflection/refraction	no	yes	yes
Number of bands implemented in ESMs	5 bands (1 visible, 4 near-IR)	3 bands (1 visible, 2 near-IR)	
Applies to	snow	bare/ponded/snow-covered sea ice, and snow	bare/ponded/snow-covered sea ice, and snow

1121